Glassy behaviour in the ferromagnetic Ising model on a Cayley tree

1996 J. Phys. A: Math. Gen. 29 5773

(http://iopscience.iop.org/0305-4470/29/18/011)

J. Phys. A: Math. Gen. **29** (1996) 5773–5804. Printed in the UK

Glassy behaviour in the ferromagnetic Ising model on a Cayley tree

R Mélin†, J C Anglès d'Auriac†, P Chandra‡ and B Douçot†

† CRTBT-CNRS, BP166X, 38042 Grenoble cédex, France
‡ NEC Research Institute, 4 Independence Way, 08540 Princeton, NJ, USA

Received 28 March 1996

Abstract. We present a detailed study of the nearest-neighbour ferromagnetic Ising model on a Cayley tree. In the limit of zero field, the system displays glassy behaviour below a crossover temperature, T_g, that scales inversely with the logarithm of the number of generations; thus T_g is inversely proportional to the logarithm of the logarithm of the number of sites. Non-Gaussian magnetization distributions are observed for $T < T_g$, reminiscent of that associated with the central spin of the Edwards–Anderson model on the same tree; furthermore, a dynamical study indicates metastability, long relaxation times and ageing consistent with the development of glassy behaviour for a finite but macroscopic number of sites.

1. Introduction

Recursive structures like the Bethe lattice and the Cayley tree provide a pedagogical environment for the study of physical problems; in this setting they can be treated with a direct analytic approach without resorting to approximate methods [1]. The Bethe lattice, an infinite Cayley tree, is a connected dendritic structure with constant coordination, z, and *no* loops, as displayed for $z = 3$ in figure 1. Strictly speaking it is a *pseudo-lattice* since it cannot be embedded in any *real* finite-dimensional lattice; indeed it is often regarded as an infinite-dimensional structure since the number of sites accessible in n steps from a given site ($\sim n^d$ for a d-dimensional lattice) increases exponentially with n. Thus the Bethe lattice provides a setting where mean-field treatments can become exact. This property was first discussed by Domb who showed that the Bethe–Peierls (BP) approximation to the nearest-neighbour (NN) ferromagnetic (FM) Ising problem, with $H = -J \sum_{(ij)} \sigma_i \sigma_j$ where $J > 0$, $\sigma_i = \pm 1$ and (ij) indicates a nearest-neighbour sum, is exact on this structure [2]; its solution is identical to that of the infinite-range FM Ising model [3]. Similarly Thouless *et al* studied the infinite-range Sherrington–Kirkpatrick (SK) model of spin glasses on the Bethe lattice using a mean-field technique [5]; they were able to recover the key results [6] of Sherrington and Kirkpatrick (SK) without using the replica method. More recently there have been several studies of the SK model on the Bethe lattice, particularly in finite fields [7–15]. In general the study of a variety of problems on this recursive structure has helped to develop our understanding of diverse physical phenomena including self-avoiding polymers [16], random resistor networks [17] and percolation [18].

Like the Bethe lattice, a Cayley tree is a connected structure with a fixed coordination number and no loops; however, it has a *finite* number of generations (cf figure 1) and hence

0305-4470/96/185773+32$19.50

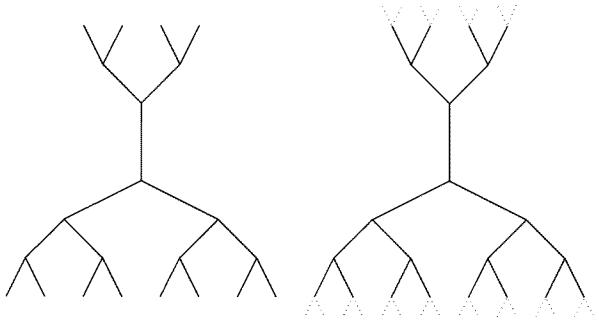

Figure 1. (*a*) A finite Cayley tree and (*b*) a section of a Bethe lattice with coordination $z = 3$.

sites that are dominated by the boundary. More specifically, the total number of sites in a Cayley tree of n generations with coordination z is

$$N = 1 + z + z(z-1) + \cdots z(z-1)^{n-1} = \frac{(z(z-1)^n - 2)}{(z-2)} \tag{1}$$

and the number of surface atoms is

$$N_s = z(z-1)^{n-1} \tag{2}$$

so that for large n

$$\lim_{n \to +\infty} \frac{N_s}{N} = \frac{(z-2)}{(z-1)} \tag{3}$$

in contrast to the situation in 'real' lattices ($\frac{N_s}{N} \sim N^{-\frac{1}{d}}$). Thus the 'surface' of a Cayley tree, in the limit of a large number of generations, contains a finite fraction of its total number of sites, and the boundary plays a key role in any problem studied on this graph. In particular, the Bethe–Peierls transition for the FM Ising model on a Cayley tree occurs *only* for its central spin; despite its finite moment, the total spontaneous magnetization of *all* the spins remains zero [20–23]. In a nutshell this occurs because at zero field and low temperatures very large domains of flipped spins can nucleate from the boundaries; the resulting finite-size glassiness is the subject of this paper.

The recursive structure of the Cayley tree permits a detailed analysis of the single-site magnetization distribution as a function of field and generation. There are two ways of handling Cayley trees. One way consists of decimating the spins on the boundary of a tree with n generations; one is left with a tree of $n-1$ generations and a magnetic field at the boundary, and one reiterates the process. This procedure is reminiscent of the Kadanoff renormalization scheme, and is implemented in section 2. Another way of treating trees is to glue together $z-1$ n-half-space trees to a common ancestor to obtain an $(n+1)$-half-space tree. By an n-half-space tree, we mean a tree of n generations such that the ancestor has $z-1$ neighbours instead of z as for a complete tree. See figure 2 for a view of how $z-1$ half-space trees are put together. Since the links are statistical independent variables, the thermodynamic properties of the $(n+1)$-half-space tree are easily expressed in terms of the thermodynamic properties of an n-half-space tree. We use this technique in section 3. In doing so, we find that for fields $h < h_{c0}$, where the crossover field h_{c0} decreases exponentially with the number of generations, there is a temperature-scale T_g below which well-defined, large domains of flipped spins exist. For $T < T_g$ the

magnetization distribution becomes non-Gaussian, reminiscent of that associated with the central spin of the magnetized spin glass phase of the $\pm J$ model on the Cayley tree. The crossover temperature, T_g, scales inversely with the logarithm of the number of generations of the Cayley tree so that the 'finite-size' glassiness persists to very large system sizes for a macroscopic number of sites.

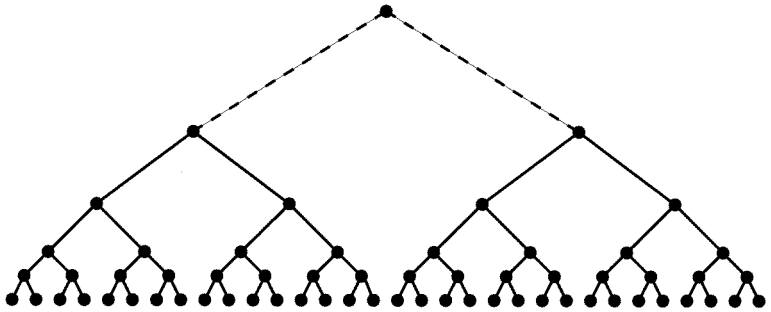

Figure 2. A recursive construction of half-space trees.

We therefore have a short-ranged spin model that has a 'glass' crossover temperature that decreases very slowly with increasing system size; more specifically it is inversely proportional to the logarithm of the logarithm of the number of sites. We characterize it using a combination of analytic and numerical techniques, always retaining open boundary conditions. First we study the magnetization for different thermodynamic limits emphasizing the crucial role of the ratio of surface/bulk sites as $n \to \infty$. We recover the Bethe–Peierls result if this ratio goes to zero; specifically for the central spin only. Otherwise, for vanishing applied fields, there is a crossover to a glassy phase characterized by well defined clusters of flipped spins. We find in that for $h < h_{c0}$, the single-site magnetization distribution becomes non-Gaussian for $T < T_g$ similar to that of spin glass models residing on the same structure; however, it recovers its Gaussian character with increasing field. For $T < T_g$ the largest barriers associated with developing broken bonds in these domains scale with the number of cluster sites; we thus refer to this low-temperature state as a finite-size glass. A dynamical study of this system, performed numerically, indicates the presence of metastable states and long relaxation times at low temperatures. The autocorrelations for $T < T_g$ are determined after a waiting time, and indicate ageing effects; the variations of χ_1' and χ_3' with temperature also agree with the presence of glassiness. As expected, the Edwards–Anderson susceptibility of the entire tree has a maximum which develops slowly with system size; no divergence is observed. We end with a summary of our results and plans for future work.

2. The different thermodynamic limits on the Cayley tree

2.1. Warm-up: the Bethe–Peierls transition of the central spin

One way to take the thermodynamic limit on an n-generation Cayley tree is to look *solely* at the properties of its central spin, and then to take the limit $n \to +\infty$. As first pointed out in [4], the behaviour of the central spin is then characteristic of an infinite-dimensional lattice; more specifically it displays a mean-field transition. In other words, the Bethe–Peierls approximation becomes exact on a finite Cayley tree if and only if one considers solely the properties of its central spin and ignores its surface. For recent results in this field, we refer the reader to reference [16]. In appendix A we give the calculation of the recursion relation

for the partition function $Z_n(\beta, H, H_n)$ of an n-generation tree with coordination z; here β is the inverse temperature and H and H_n are the magnetic fields acting on the spins of generations 0 to $n-1$ and n respectively. The resulting recursion relation for $Z_n(\beta, H, H_n)$ is

$$Z_n(\beta, h, h_n) = (4(\cosh^2(\beta J) + \sinh^2(\beta h_n))^{(z-1)^n/2} Z_{n-1}(\beta, h, h + Th_n) \quad (4)$$

where the transformation of the magnetic field is

$$Th = \frac{z-1}{2\beta} \ln \frac{\cosh \beta(J+h)}{\cosh \beta(J-h)}. \quad (5)$$

We consider the special case of a small field ϵ applied at the surface of a tree, and ask whether it is amplified in the bulk as determined by the recursion relation (5). This condition defines the bulk critical temperature β_c by the expression $(z-1)\tanh \beta_c J = 1$. If $\beta < \beta_c$, the magnetization of the central spin is zero; however if $\beta > \beta_c$, there is a broken symmetry for the central spin in the thermodynamic limit. As discussed in [3], the critical behaviour of the central spin in the thermodynamic limit is identical to that of an infinite-range ferromagnet where $\beta' = \frac{1}{2}$ and $\delta = 3$. Note here that we use β' to distinguish from the inverse temperature.

2.2. Beyond the Bethe–Peierls regime: different thermodynamic limits

We now wish to look at the transition, not only of the central spin, but of the entire tree. First we consider only *half-space trees*, that is trees such that the coordination associated with the ancestor is $z-1$ and not z. We shall label the generations so that the ancestor is at generation n and the leaves are at generation 0. We are interested in the magnetic properties of the spins in generations $n-m$ to n in the limit $n \to +\infty$ where, of course, m is a function of n; more specifically we want to classify the different regimes as a function of $m(n)$ in an external uniform field h. In order to obtain the magnetization of the generations $n-m$ to n, we must apply a source magnetic field λ to these generations; then we differentiate the partition function with respect to λ in the limit $\lambda \to 0$ to obtain

$$\langle M(n, m, h)\rangle = \frac{\partial}{\partial(\beta\lambda)} \ln Z(n, m, h, \lambda = 0). \quad (6)$$

Details of the calculation are provided in appendix B. There exist two regimes for the iteration of the magnetic field: $i < n_c(h)$ and $i > n_c(h)$, where $n_c(h)$ is given by equation (B8) and i is the distance from the boundary. We thus have to distinguish between three regimes: $0 \leqslant n_c \leqslant n-m$ (regime (I)), $n-m+1 \leqslant n_c \leqslant n$ (regime (II)) and $n_c \geqslant n$ (regime (III)).

2.2.1. Regime I: $0 \leqslant n_c \leqslant n-m$—large fields. The details of the calculation are given in appendix B. We obtain that, in this regime, the magnetization per site between the generations $n-m$ and n tends to a constant in the thermodynamic limit

$$\lim \frac{\langle M(n, m, h)\rangle}{N_m} = \left(b_2 + a_2 \frac{h}{\eta_2}\right) \frac{z-1}{z-2+\eta_2} \quad (7)$$

where a_2 and b_2 are related to the temperature (see (B15) and (B16)).

2.2.2. Regime II: $n - m + 1 \leqslant n_c \leqslant n$—intermediate fields. In this regime, we find that if $T' < T < T_c$, the dominant term in the normalized magnetization is proportional to the magnetic field h, with corrections proportional to h^α, where the exponent α is given in appendix B. The temperature T' is defined by $\tanh(\beta' J) = 1/\sqrt{z-1}$. In the temperature regime where $T < T'$, the leading term of the magnetization is of order h^α.

2.2.3. Regime III: $n_c \geqslant n$—vanishing fields. We show in appendix B that, if $T > T'$, the susceptibility per spin tends to a constant as $n \to +\infty$, $m \to +\infty$ and $n - m$ is constant. In the regime where $T < T'$, the susceptibility per spin is proportional to

$$\chi(m) \propto (z-1)^m (1 - 4m\mathrm{e}^{-2\beta J}). \tag{8}$$

If $T > T_g = 2J/\ln m$, the critical behaviour is cut-off, whereas if $T < T_g$, the susceptibility per spin is critical. The crossover temperature T_g is rederived by different methods in what follows.

2.3. Correlation length

The aim of this section is to calculate the size above which the central spin is decorrelated from the boundary spin in a zero magnetic field. This is another way of calculating T_g. If the system size is smaller than this typical size, the system is critical. The two points correlation $\langle \Sigma\sigma \rangle$ is

$$\langle \Sigma\sigma \rangle = \sum_{k=0}^{n} \binom{n}{k} (-x)^k (1-x)^{n-k} = (1-2x)^n \simeq 1 - 2nx \tag{9}$$

where Σ is the spin of the ancestor and σ is the spin variable on the leaf. x is the probability that two neighbouring spins are antiparallel:

$$x = \frac{\mathrm{e}^{-\beta J}}{\mathrm{e}^{\beta J} + \mathrm{e}^{-\beta J}}. \tag{10}$$

The system is thus critical provided $nx \ll 1$, that is $T < T_g \simeq J/n$.

3. Magnetization distribution and finite-size effects

Next, we study the distribution of the magnetization which can be determined from exact recursion relations. We find that finite-size effects are crucial in this analysis, and we recover the crossover temperature T_g discussed in the previous section. We also compute the distribution of the magnetization in finite field.

3.1. Magnetization distribution in zero field

We begin with the case of zero magnetic field. Given $z-1$ n-half-space trees with coordination z, it is straightforward to obtain an $(n+1)$-half-space tree with the same coordination. One just has to add a common ancestor and to link it to the $z-1$ ancestors of each n-tree (see figure 2). In order to get a full tree, one has to 'glue' z half-space trees instead of $z-1$ at the last step. Let $P_n^\sigma(M)$ be the conditional probability for an n-half-space tree to have a magnetization M, given that the spin of the ancestor is σ. Of course,

$$\sum_M P_n^\sigma(M) = 1. \tag{11}$$

The recursion relation for $P_n^\sigma(M)$ is

$$P_n^\sigma(M) = \sum_{M_1,\ldots,M_{z-1}} \delta(M-(M_1+\cdots+M_{z-1}+\sigma)) \sum_{k=0}^{z-1} \binom{k-1}{k} x^k (1-x)^{z-k-1} \times \prod_{i=1}^{k} P_{n-1}^{-\sigma}(M_i) \prod_{i=k+1}^{z-1} P_{n-1}^{\sigma}(M_i) \tag{12}$$

where x is the probability for breaking one bond. The initialization of the recursion is given by $P_1^\sigma(\sigma') = \delta_{\sigma,\sigma'}$. This recursion can be performed numerically, at least for a small number of generations. The result is plotted in figure 4 for $z = 3$ and 10 generations. For a finite-size tree and at low temperature, the magnetization distribution presents a non-Gaussian structure, reminiscent of the magnetization distribution of the central spin in Bethe lattice spin glasses [10, 14]. Notice that the temperature which controls the departure from the Gaussian distribution is lower than the bulk transition temperature.

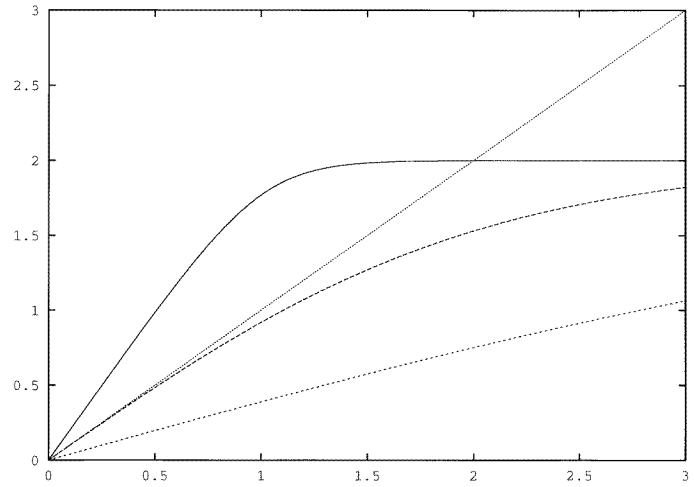

Figure 3. $h_{i+1}^{ind}(h_i)$ where h_i is the total magnetic field at generation i, and h_{i+1}^{ind} is the iterated field of equation (5). From bottom to top, the curves correspond to $\beta < \beta_c$, $\beta = \beta_c$ and $\beta > \beta_c$.

In order to determine precisely this temperature, we compute the recursion relations for the average magnetization. Using the recursion relations (12), we find

$$\langle M\rangle_{n+1}^{+} = 1 + \sum_{k=0}^{z-1} \binom{z-1}{k} x^k (1-x)^{z-k-1} (k\langle M\rangle_n^{-} + (z-k-1)\langle M\rangle_n^{+}). \tag{13}$$

It is clear that, since $P_1^+(\sigma) = P_1^-(-\sigma)$, for all n, $P_n^+(M) = P_n^-(-M)$, so that $\langle M\rangle_n^+ + \langle M\rangle_n^- = 0$. Putting this equation into (13) and using the well known relations for the sum of binomial series, we obtain $\langle M\rangle_{n+1}^+ = p\langle M\rangle_n^+ + 1$ and $\langle M\rangle_0^+ = 1$ where p is defined as $p = (z-1)\tanh\beta J$. This recursion can be easily solved, and one gets

$$\frac{\langle M\rangle_n^+}{N_n} = \frac{z-2}{p-1}\frac{p^{n+1}-1}{(z-1)^{n+1}-1} \tag{14}$$

where N_n is the number of sites of an n-half-space tree, given by (B17). The structure of the distribution of magnetization is non-Gaussian provided $2x^2 n \ll 1$, that is

$$T < T_g = \frac{2J}{\ln n} = \frac{2J}{\ln(\ln N_n/\ln(z-1))}. \tag{15}$$

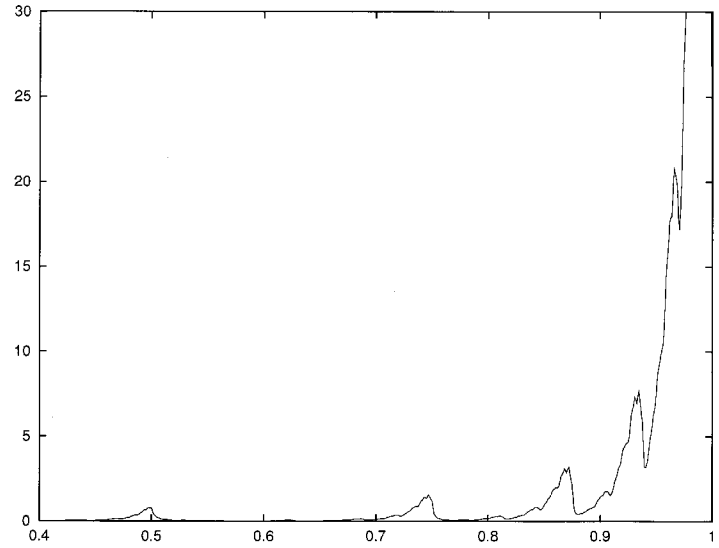

Figure 4. The probability density of the magnetization on a half-space tree where $n = 10$, $z = 3$, the ancestral spin is fixed, and the inverse temperature is $\beta = 3$.

It is clear that the temperature T_g (which will be identified with the glass temperature) decreases very slowly with the system size. For instance, in limit where $N \simeq 6.02 \times 10^{23}$ and $z = 3$, $T_g = J/4.4$. We conclude from this analysis that finite-size effects persist in the limit of a macroscopic number of sites. For T_g to be drastically reduced, one should consider systems of size $\exp(6.02 \times 10^{23})$(!). Since the appearance of glassiness is a finite-size effect, we stress that T_g is a *crossover* temperature scale even for macroscopic systems.

3.2. Structure of the magnetization distribution for $T < T_g$

We would like to understand qualitatively the structure of the maxima of the magnetization probability distribution below T_g; more specifically we want to localize the maxima and calculate their weight. To do this, we use the normalized continuous magnetization variable $m = M/N_n \in [-1, 1]$ and the associated density $\rho_n(m) = N_n P_n^+(M)$. The recursion relations for $\rho_n(m)$ are derived in a straightforward fashion from those for $P_n^+(M)$ that are shown in (12). Since this relation is a convolution, we write the recursion in terms of the Fourier transform $\tilde{\rho}_n(k)$ of $\rho_n(m)$:

$$\tilde{\rho}_n(k) = \int_{-\infty}^{+\infty} \mathrm{e}^{\mathrm{i}km} \rho_n(m)\, \mathrm{d}m \tag{16}$$

where we have neglected the contribution of the ancestor. That is, we assumed that $N_{n+1} \simeq (z-1)N_n$. We obtain the recursion of the $\tilde{\rho}$s:

$$\tilde{\rho}_{n+1}(k) = \left(x\tilde{\rho}_n\left(-\frac{k}{z-1}\right) + (1-x)\tilde{\rho}\left(\frac{k}{z-1}\right)\right)^{z-1} \tag{17}$$

$$\tilde{\rho}_0(k) = \mathrm{e}^{\mathrm{i}k}. \tag{18}$$

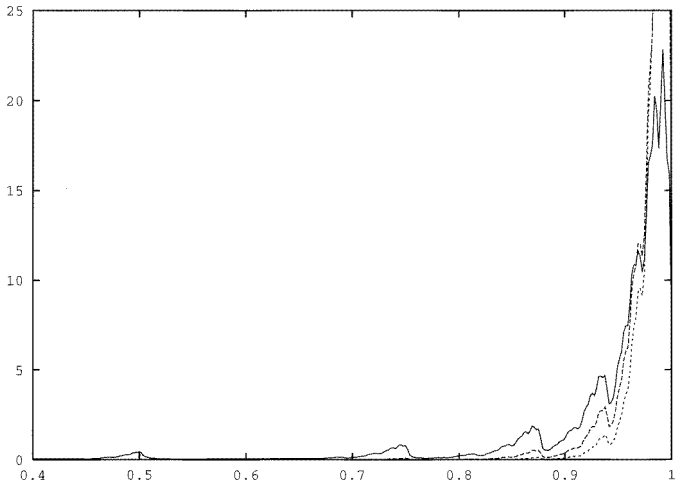

Figure 5. The conditional magnetization distribution in the presence of a magnetic field, the field being parallel to the central spin. The magnetization distribution is plotted for a $z = 3$ tree, $n = 10$ generations, and for magnetic fields $H = 0$, 0.001, 0.002. The magnetization distribution evolves towards a Gaussian shape as the magnetic field increases.

We now study the special case $z = 3$ where the formulae are simpler. It is easy to check by recursion that

$$\tilde{\rho}_n(k) = (1 - 2x(2^n - 1))\mathrm{e}^{\mathrm{i}k} + 2x \sum_{\alpha=0}^{n-1} 2^\alpha \exp\left(\mathrm{i}\left(1 - \frac{1}{2^\alpha}\right)k\right) + \mathrm{O}(x^2). \tag{19}$$

As we shall see later, this low-temperature expansion is meaningful below T_g even in the presence of a finite density of kinks. The expansion (19) tells us that $\rho_n(m)$ has peaks for $m_\alpha = 1 - 1/2^\alpha$, where $\alpha \in \langle 0, \ldots, n-1 \rangle$. Moreover, we find that the weight of the peak $\alpha + 1$ is twice that of α. Inspection of figure 4 indicates that this prediction is correct, at least in the region where the overlap between the peaks is small.

These results can also be interpreted in the following fashion. The expansion (19) at order x means that the magnetization density is calculated at the order of one kink. It is clear that a single kink at generation $n - \alpha$ leads to a magnetization $1 - 1/2^\alpha$ and that the number of choices to put a kink at generation $n - \alpha - 1$ is twice the number of choices to put a kink at generation $n - \alpha$, which is the content of equation (19). What is striking is that below T_g, this one kink picture is valid, even though we deal with a finite density of kinks x. This means that T_g is the temperature below which the kinks are rarely nested. In order to check this assertion, we determine the condition for the kinks to 'induce' well-defined domains of flipped spins; this criterion will determine the validity of the expansion (19). The overlap between the domains induced by the kinks is small provided $xN_n\langle S\rangle_n < N_n$. In this expression, $\langle S\rangle_n$ is the average size of a domain of flipped spins induced by a single kink. The number of descendants of a kink at level $n - p$ for an n-half-space tree is $S_{p,n} = 1 + 2 + \cdots + 2^{n-p} = 2^{n-p+1} - 1$. The average over p of $S_{p,n}$ is

$$\langle S_{p,n}\rangle_n = \frac{\sum_{p=1}^n 2^p S_{p,n}}{\sum_{p=1}^n 2^p} = n\frac{2^n}{2^n - 1} - 1 \simeq n - 1. \tag{20}$$

The condition for 'non-overlap' is $xn < 1$ which is just $T < T_g$. We conclude that for $T < T_g$, the number of kinks is small enough for the system to develop well-defined domains

of flipped spins. In this temperature regime, the excitations of the spin system are kinks which are local in the bond variables but are *highly* non-local in terms of the spins.

3.3. Magnetization distribution in a magnetic field

The magnetization distribution in a magnetic field can be computed using

$$P^{\sigma}_{n,h}(m) = \frac{P^{\sigma}_{n,0}(m)\mathrm{e}^{\beta m h}}{\sum_{m'} P^{\sigma}_{n,0}(m')\mathrm{e}^{\beta h m'}}. \tag{21}$$

The conditional magnetization distribution (the central spin being parallel to the field) is found to converge rapidly to a Gaussian as the field increases. Since large domains of flipped spins do not survive in a magnetic field, the crossover field is expected to decrease drastically with the system size. Indeed, we have shown previously that the crossover field h_{c0} of equation (B28) decreases exponentially with the number of generations. The distribution of magnetizations is plotted on figure 5, where the central spin is taken to be parallel to the field.

4. Conclusion on the thermodynamics

We have thus shown the existence of a temperature $2J/n$ below which the susceptibility per spin is critical (section 2.2.3). Below a temperature of the order $J/\ln n$, the spin system is critical in the sense that the ancestor tends to point in the same direction as the spin on the leaves (section 2.3). By calculating the magnetization of the spin system, we have shown that the spin system is magnetized below a crossover temperature of the order $2J/\ln n$ (section 3). The condition for non-overlap of domains leads to a temperature scale $J/\ln n$ below which the domains are weakly overlapping. We call T_g the temperature scale $T_g \sim J/\ln n$. From the analysis of the ferromagnetic Ising model on fractals and percolation clusters [18], where the system is also critical below $T_g \sim 1/\ln N_n$, we expect that the dynamics is also critical below T_g, with the existence of a glassy-like relaxation. We now study the dynamics of the Ising model on the Cayley tree at low temperatures.

5. Barrier structure

Since a glass transition or a glass crossover is dynamical in nature, we first study the energy barriers. We have shown that the excitations below T_g are broken bonds. In order to characterize the dynamics, we calculate the barriers associated with these excitations. The energy barriers at zero temperature of a half-space tree are defined as follows. One starts with a configuration where all the spins are up and then one considers single-spin-flip paths from the initial configuration to a final one where all the spins are reversed. To each such single-spin-flip path, we associate the maximal energy reached during the 'passage' from the initial to the final configuration where we take the energy of the former to be zero. Then the barrier is defined as the minimum over all the paths of the maximum energy of one path. Typically, the Monte Carlo algorithm samples all the paths in an ergodic way; by contrast the Swendsen–Wang algorithm [19] does not generate paths with respect to the single flip. In appendix C we give details of the calculation of the barriers associated with the n-half-space tree. Here we calculate the number of states with a given barrier E^{b}_{α} at a given temperature below T_g, for a full n-tree. Following our previously established convention, the leaves and the centre reside at the first and the nth generation respectively. We note there exist n^* kinks at a given temperature where $n^* = Nx$. The barrier for a

configuration of n^* kinks is assumed to be only a function of the generation α of the kink which is closest to the origin. In order to calculate the number of states with an energy barrier E_α^b, we have to enumerate all the configurations with no kink between generation $\alpha+1$ and n, n_α kinks at generation α and n^*-n_α kinks between generations $\alpha-1$ and 1. We call the number of such configurations of kinks $g(\alpha)$. We make the approximation that the energy barrier of all these configurations is E_α^b so that its lifetime is, according to the Arrhenius law,

$$\tau_\alpha = \tau_0 \exp(\lambda\beta E_\alpha^b) \tag{22}$$

where λ is a constant. Such a configuration of kinks is displayed in figure 6. Clearly, we have

$$g(\alpha) = \sum_{n_\alpha=1}^{n^*} g_\alpha(n_\alpha) \tag{23}$$

with

$$g_\alpha(n_\alpha) = \binom{z(z-1)^{n-\alpha-1}}{n_\alpha}\binom{\frac{z}{z-2}((z-1)^{n-1}-(z-1)^{n-\alpha})}{n^*-n_\alpha}. \tag{24}$$

We can calculate the sum and obtain

$$g(\alpha) = \binom{\frac{z}{z-2}((z-1)^{n-1}-(z-1)^{n-\alpha-1})}{n^*} - \binom{\frac{z}{z-2}((z-1)^{n-1}-(z-1)^{n-\alpha})}{n^*} \tag{25}$$

and we get the probability $P(\alpha)$ for the system to be in a valley with a barrier E_α:

$$P(\alpha) = \binom{N}{Nx}^{-1}\left[\binom{N(1-(z-1)^{-\alpha})}{Nx} - \binom{N(1-(z-1)^{-\alpha+1})}{Nx}\right] \tag{26}$$

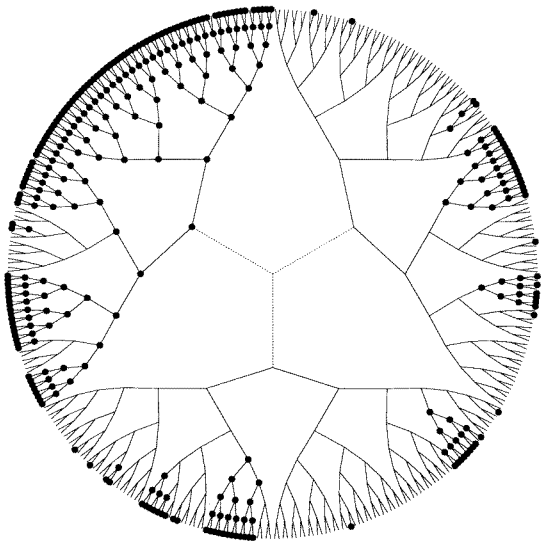

Figure 6. A typical configuration of the tree with $n = 8$ and $\beta = 1.5$. The vertices with no dots represent up spins and the dots represent flipped spins. Each kink gives rise to a well-defined domain of flipped spins.

where we have normalized by the total number of accessible states at a given temperature on an n-tree. We have also approximated the number of sites as follows:

$$N = \frac{z(z-1)^{n-1}-2}{z-2} \simeq \frac{z(z-1)^{n-1}}{z-2}. \tag{27}$$

Assuming both that $x \ll 1$, and that $(z-1)^{-\alpha} \ll 1$, and using Stirling's formula, we get

$$P(\alpha) \simeq \exp\left(-\frac{Nx}{(z-1)^{\alpha}}\right) - \exp\left(-\frac{Nx}{(z-1)^{\alpha-1}}\right). \tag{28}$$

If $Nz/(z-1)^{\alpha} \ll 1$, we obtain

$$P(\alpha) \simeq Nx\frac{z-2}{(z-1)^{\alpha}}. \tag{29}$$

As expected, $P(\alpha)$ decreases as a function of α, which indicates that the long-lived states are less numerous than their short-lived counterparts. At low temperatures, there is thus a hierarchy of relaxation times.

6. Glauber dynamics

We now study the Glauber dynamics of the spin system on the Cayley tree.

6.1. The Glauber matrix

We begin with a general discussion of Glauber dynamics. Let $p(\{\sigma\}, t)$ be the probability for the system to be in a state $\{\sigma\}$ at time t. Following Glauber [24], we define $w_i(\{\sigma\})$ as the probability per unit time that the spin i flips from σ_i to $-\sigma_i$, while the others remain fixed. The master equation is

$$\begin{aligned}\frac{\mathrm{d}}{\mathrm{d}t}p(\{\sigma\},t) = &-\left(\sum_{i=1}^{N} w_i(\{\sigma\})\right)p(\{\sigma\},t) \\ &+\sum_{i=1}^{N} w_i(\{\sigma_1,\ldots,-\sigma_i,\ldots,\sigma_N\})p(\{\sigma_1,\ldots,-\sigma_i,\ldots,\sigma_N\},t).\end{aligned} \tag{30}$$

Since we require the Boltzmann distribution to be a fixed point, the coefficients $w_i(\{\sigma\})$ are of the form

$$w_i(\{\sigma\}) = \tfrac{1}{2}\left(1 - \sigma_i \tanh\left(\beta J \sum_{j\in V(i)} \sigma_j\right)\right) \tag{31}$$

where $V(i)$ is the set of neighbours of the site i. If one denotes by $\boldsymbol{p}(t)$ the 2^N vector of $p(\{\sigma\}, t)$, equation (30) can be written as

$$\frac{\mathrm{d}}{\mathrm{d}t}\boldsymbol{p}(t) = \mathbf{G}\boldsymbol{p}(t) \tag{32}$$

where $\mathbf{G}$ is the Glauber matrix. We first show some properties of the matrix $\mathbf{G}$. Since the Boltzmann distribution is a steady state of the dynamics, its corresponding eigenvalue is zero whatever the temperature. Even though it is *not* symmetric, the matrix $\mathbf{G}$ can be diagonalized and its eigenvalues are real; we give the proof of this statement here. The Glauber matrix satisfies a detailed balance which means that $\mathbf{G}_{\alpha,\beta}\boldsymbol{p}^{(0)}_{\beta} = \mathbf{G}_{\beta,\alpha}\boldsymbol{p}^{(0)}_{\alpha}$ where $\boldsymbol{p}^{(0)}$ is the Boltzmann distribution. As a consequence

$$(\boldsymbol{p}^{(0)}_{\alpha})^{-1/2}\mathbf{G}_{\alpha\beta}(\boldsymbol{p}^{(0)}_{\beta})^{1/2} = (\boldsymbol{p}^{(0)}_{\beta})^{-1/2}\mathbf{G}_{\beta\alpha}(\boldsymbol{p}^{(0))}_{\alpha})^{1/2}. \tag{33}$$

Let us define a matrix $\mathbf{M}$ such that

$$\mathbf{M}_{\alpha\beta} = (\boldsymbol{p}_\alpha^{(0)})^{-1/2}\mathbf{G}_{\alpha\beta}(\boldsymbol{p}_\beta^{(0)})^{1/2}. \tag{34}$$

Then $\mathbf{M}$ is symmetric. Let $\boldsymbol{p}$ be a right eigenvector of the Glauber matrix. Then

$$\sum_\beta \mathbf{G}_{\alpha\beta}\boldsymbol{p}_\beta = \lambda \boldsymbol{p}_\alpha \tag{35}$$

is equivalent to

$$\sum_\beta \mathbf{M}_{\alpha\beta}(\boldsymbol{p}_\beta^{(0)})^{-1/2}\boldsymbol{p}_\beta = \lambda(\boldsymbol{p}_\alpha^{(0)})^{-1/2}\boldsymbol{p}_\alpha \tag{36}$$

so that $(\boldsymbol{p}_\alpha^{(0)})^{-1/2}\boldsymbol{p}_\alpha$ is an eigenvector of $\mathbf{M}$. We conclude that $\mathbf{G}$ is diagonalizable, and that all of its eigenvalues are real.

The spectrum in the infinite temperature limit can be understood in the following manner. If we define a state vector $|\psi\rangle$ by

$$|\psi\rangle = \sum_{\{\sigma\}} f((\{\sigma\})|\sigma_1\rangle \otimes \cdots \otimes |\sigma_N\rangle \tag{37}$$

then its dynamics are

$$\frac{\mathrm{d}}{\mathrm{d}t}|\psi\rangle = -\frac{N}{2}|\psi\rangle + \frac{1}{2}\sum_{i=1}^{N}\sigma_i^x|\psi\rangle \tag{38}$$

so that the eigenvalues of the Glauber matrix at infinite temperature are of the form

$$\lambda = -\frac{N}{2} + \frac{1}{2}\sum_{i=1}^{N}\mu_i \tag{39}$$

where $\mu_i = \pm 1$. The spectrum in the infinite temperature limit is composed of levels at integer values between $-N$ and 0, with a degeneracy given by the binomial coefficients.

For bipartite lattices, such as the square lattice of the Cayley tree, the spectrum of the matrix $\mathbf{G}$ is symmetric; more specifically if λ belongs to the spectrum, then $-N-\lambda$ is an eigenvalue too. We give the proof of this statement now. Let $\boldsymbol{X}\{\sigma\}$ be an eigenvector of $\mathbf{M}$, with an eigenvalue λ:

$$\lambda \boldsymbol{X}\{\sigma\} = -\sum_{i=1}^{N}\frac{1}{2}(1-\sigma_i\tanh(\beta J h_i))\boldsymbol{X}\{\sigma\} + \sum_{i=1}^{N}\frac{1}{2\cosh\beta J h_i}\boldsymbol{X}\{\sigma_1,\ldots,-\sigma_i,\ldots,\sigma_N\} \tag{40}$$

where h_i is defined by

$$h_i = \sum_{j\in V(i)}\sigma_j. \tag{41}$$

Let $\boldsymbol{Y}\{\sigma\}$ be defined as

$$\boldsymbol{Y}\{\sigma\} = (-1)^{\nu\{\sigma\}}\boldsymbol{X}\{\tilde{\sigma}\} \tag{42}$$

where $\nu\{\sigma\}$ is the number of up spins in the configuration $\{\sigma\}$. $\{\tilde{\sigma}\}$ is deduced from $\{\sigma\}$ by flipping the spins of one of the two sublattices. Then,

$$\begin{aligned}(\mathbf{M}\boldsymbol{Y})\{\sigma\} = &-\sum_{i=1}^{N}\tfrac{1}{2}(1-\sigma_i\tanh(\beta H h_i))(-1)^{\nu\{\sigma\}}\boldsymbol{X}\{\tilde{\sigma}\} \\ &+\sum_{i=1}^{N}\frac{(-1)^{\nu\{\sigma_1,\ldots,-\sigma_i,\ldots,\sigma_N\}}}{2\cosh(\beta J h_i)}\boldsymbol{X}\{\tilde{\sigma}_1,\ldots,-\tilde{\sigma}_i,\ldots,\tilde{\sigma}_M\}\end{aligned}$$

$$= (-1)^{\nu\{\sigma\}}\Big[-\sum_{i=1}^{N} \tfrac{1}{2}(1+\tilde{\sigma}_i \tanh(\beta J h_i))\boldsymbol{X}\{\tilde{\sigma}\}$$

$$-\sum_{i=1}^{N} \frac{1}{2\cosh(\beta J h_i)} \boldsymbol{X}\{\tilde{\sigma}_1, \ldots, -\tilde{\sigma}_i, \ldots, \tilde{\sigma}_N\}\Big] \tag{43}$$

$$= -(N+\lambda)(-1)^{\nu\{\sigma\}}\boldsymbol{X}\{\tilde{\sigma}\} = -(N+\lambda)\boldsymbol{Y}\{\sigma\}. \tag{44}$$

Given an eigenvector $\boldsymbol{X}$ for the eigenvalue λ, we have constructed an eigenvector $\boldsymbol{Y}$ for the eigenvalue $-N-\lambda$.

The difference between (32) and the Schrödinger equation is that quantum mechanics preserves the scalar product which results in Hermitian Hamiltonians. Furthermore, the physical states 'reside' in a Hilbert space, and each state of this Hilbert space is physical. In the case of the Glauber matrix there is no such vectorial space; more specifically, the sum of two probability distributions is not a probability distribution. However, some quantities are conserved by the dynamics. It is easy to show that the eigenvectors of **G** for the non-zero eigenvalues have the property that

$$\sum_{\{\sigma\}} \boldsymbol{p}\{\sigma\} = 0. \tag{45}$$

This is a simple consequence of the fact that the Glauber matrix preserves the quantity

$$\sum_{\{\sigma\}} \boldsymbol{p}\{\sigma\}. \tag{46}$$

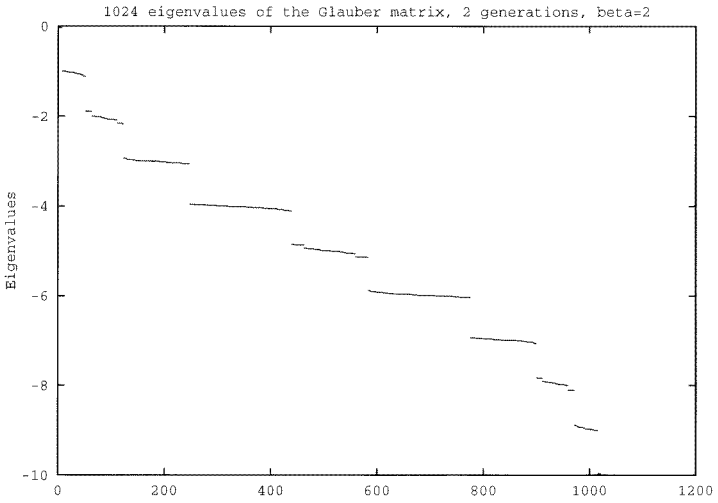

Figure 7. Spectrum of the Glauber matrix at a given temperature for a $z = 3$ Cayley tree with two generations. The inverse temperature is $\beta = 2$. The spectrum is symmetric with respect to the $\lambda = -N/2$ line. The clusters collapse at integer values.

6.2. Spectrum of the Glauber matrix at low temperature

The spectrum of the Glauber matrix at low temperature is plotted in figure 7. We see that the eigenvalues collapse around integers. The reason why this is the case is that, in the case $z = 3$, the local field never vanishes on any site. Since the extra diagonal coefficients have

the form $1/\cosh(\beta h_i)$, where h_i is the local field on site i, the Glauber matrix is diagonal in the zero temperature limit, with integer coefficients. This property is also valid on any graph for disordered systems, where the local field also never vanishes. For a detailed study of the spectral properties of the Glauber matrix, see [25].

6.3. Realization of the Glauber dynamics

We now diagonalize the Glauber matrix in order to determine the dynamics of the model in an explicit fashion. Let $\boldsymbol{u}_\alpha$ be the eigenvectors of $\mathbf{G}$: $\mathbf{G}\boldsymbol{u}_\alpha = \lambda_\alpha \boldsymbol{u}_\alpha$, and let $\mathbf{P}$ be the passage matrix from the natural basis of pure states $\boldsymbol{e}_\alpha$ to the basis $\boldsymbol{u}_\alpha$:

$$\boldsymbol{u}_\alpha = \sum_\beta \mathbf{P}_{\alpha\beta}\boldsymbol{e}_\beta. \tag{47}$$

We look for the temporal evolution of the states $\boldsymbol{e}_\alpha$. At the initial time ($t = 0$)

$$\boldsymbol{p}_\alpha(0) = \boldsymbol{e}_\alpha = \sum_\beta \mathbf{P}^{-1}_{\alpha\beta}\boldsymbol{u}_\beta \tag{48}$$

and at $t > 0$, the state is a mixture of pure states and is given by

$$\boldsymbol{p}_\alpha(t) = \sum_\beta \mathbf{P}^{-1}_{\alpha\beta} \mathrm{e}^{\lambda_\beta t} \sum_\gamma \mathbf{P}_{\beta\gamma}\boldsymbol{e}_\gamma. \tag{49}$$

We can easily compute the magnetization of $\boldsymbol{p}_\alpha(t)$. We applied this procedure to the case of a tree with one generation. The evolution of the magnetization of the 16 pure states is plotted in figure 8 at low temperature. Of course, on very long time scales, the magnetization of all the states relaxes to zero, due to the fact that the eigenvalues associated with the symmetry-breaking state are not strictly zero. The evolution of the pure states indicates the existence of metastable states, which are the precursors of the metastable states present for larger values of the number of generations.

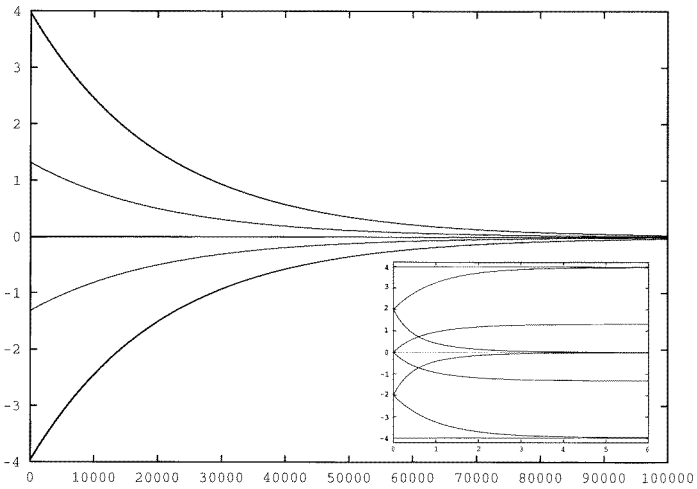

Figure 8. Evolution of the magnetization of the 16 pure states of the tree with one generation. The inverse temperature is $\beta = 3$. Metastable states appear to be present even for such a small size. The insert represents the same curve at short time scales, which shows the transient regime from the natural basis of pure states to the metastable states.

6.4. The factorization approximation

We recover the bulk critical temperature by considering the asymptotics of a simplified Glauber dynamics. Glauber has shown [24] that one can replace the 2^N variables of the linear dynamics by a hierarchy of N, nonlinear, coupled equations for the correlation functions. This procedure is very similar to the transformation of the Liouville equation into the BBGKY hierarchy in the kinetic theory. The first equation of the hierarchy is

$$\frac{\mathrm{d}}{\mathrm{d}t}q_i(t) = -q_i(t) + \left\langle \tanh\left(\beta J \sum_{j\in V(i)} \sigma_j\right)\right\rangle. \tag{50}$$

In this expression, $q = \langle\sigma\rangle$ and $V(i)$ is the set of neighbours of site i. In the case of a one-dimensional chain, one can use the fact that

$$\langle \tanh \beta J(\sigma_{i-1} + \sigma_{i+1})\rangle = \tfrac{1}{2}\tanh(\beta J)(q_{i-1} + q_{i+1}) \tag{51}$$

and one gets a closed equation for the one-point correlation functions. It is also clear that the whole hierarchy decouples, and that one can use this decoupling to integrate the dynamics. In the case of a $z = 3$ tree, one has to take into account the fact that the sites inside the tree have three neighbours; by contrast the leaves have one neighbour. For this coordination,

$$\tanh \beta J(\sigma_1 + \sigma_2 + \sigma_3) = \alpha(\sigma_1 + \sigma_2 + \sigma_3) + \gamma(\sigma_1 + \sigma_2 + \sigma_3)^3 \tag{52}$$

where the coefficients α and γ are determined by

$$\alpha = \tfrac{1}{24}(27\tanh\beta J - \tanh 3\beta J) \tag{53}$$

$$\gamma = \tfrac{1}{24}(\tanh 3\beta J - 3\tanh\beta J). \tag{54}$$

We can thus obtain the first equation of the hierarchy in the case of the $z = 3$ tree. For the sites with three neighbours,

$$\frac{\mathrm{d}}{\mathrm{d}t}q_i = -q_i + (\alpha + 7\gamma)\sum_{j\in V(i)} q_j + 6\gamma\left\langle \prod_{j\in V(i)} \sigma_j\right\rangle. \tag{55}$$

For the leaves of the tree

$$\frac{\mathrm{d}}{\mathrm{d}t}q_i = -q_i + q_j \tanh\beta J \tag{56}$$

where j is the neighbour of i. The factorization approximation consists in decoupling the third-order correlations into

$$\left\langle \prod_{j\in V(i)} \sigma_j\right\rangle = \prod_{j\in V(i)} q_j. \tag{57}$$

This approximation leads to the bulk behaviour in the high temperature phase and in the vicinity of the transition. We start from a configuration of spins such that $q_i(0) = q_j(0)$ if the sites i and j belong to the same generation. Then, for $t > 0$, $q_i(t) = q_j(t)$ if we work with the factorized dynamics. The factorized dynamics depends only on n variables, one per generation, and is

$$\begin{aligned}
\frac{\mathrm{d}q_n}{\mathrm{d}t} &= -q_n + 3(\alpha + 7\gamma)q_{n-1} + 6\gamma q_{n-1}^3 \\
\frac{\mathrm{d}q_i}{\mathrm{d}t} &= -q_i + (\alpha + 7\gamma)(2q_{i-1} + q_{i+1}) + 6\gamma q_{i-1}^2 q_{i+1} \\
\frac{\mathrm{d}q_1}{\mathrm{d}t} &= -q_1 + q_2\tanh\beta J
\end{aligned} \tag{58}$$

where i runs from 2 to $n-1$. The equilibrium properties are calculated from the asymptotic values of the dynamics. We note that the factorized dynamics possesses a non-trivial fixed point for a finite-size system, whereas the complete dynamics possesses only the Boltzmann distribution as a fixed point. The asymptotics of the factorized dynamics is found to reproduce quite well the bulk properties of the tree. In figure 9, $q_n(+\infty)$ is plotted as a function of the inverse temperature. This curve is in agreement with the fact that the central spin exhibits a mean-field-like transition at $\beta_c \simeq 0.54$. We also plotted the asymptotic magnetization of the m generations which are closest to the central spin. It is clear that the predictions of the factorized dynamics are qualitatively wrong as soon as one goes out from the centre. For instance, it is clear that the entire tree does not develop a transition at $\beta = \beta_c$. We note that, in equations (58), the transition temperature is determined entirely by the stability of the zero fixed point of the linear problem. Below T_c, the largest eigenvalue of the linear problem is positive, and negative above T_c. As the Ginzburg–Landau theory, the nonlinear terms are responsible for the maximum bound on the dynamical variables in the low-temperature phase.

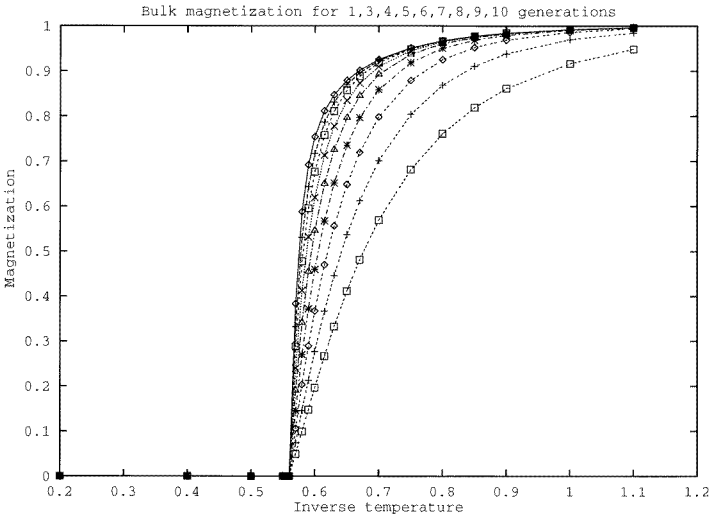

Figure 9. Expectation value of the central spin in the simplified dynamics, as a function of the inverse temperature. The transition temperature is in agreement with the value $\beta_C \simeq 0.54$. The shape of the curve near the transition is in agreement with the existence of a mean-field-like transition for the central spin. We also plotted the expectation value of the magnetization of the m closest to the origin slices of spins, in the factorization approximation, for $m = 3$, 4, 5, 6, 7, 8, 9, 10.

7. Monte Carlo dynamics

7.1. Relaxation of a single kink

We begin by considering the case of a single kink and look for the relaxation of this excitation at low temperatures. Let us call K the set of descendants of the kink. At time $t = 0$, the configuration of kinks is such that $\sigma_i = -1$ is $i \in K$ and $\sigma_i = 1$ if $i \notin K$. We follow the magnetization of the spins of K as a function of time, for various sizes of K. The result is plotted in figure 10. The rapid relaxation at small times is attributed

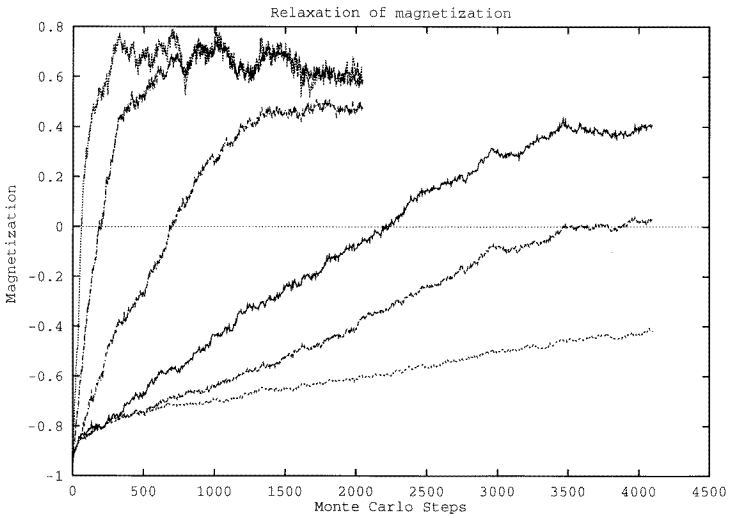

Figure 10. Magnetization relaxation of a single kink. Initially, all the spins of a $z = 3$, $n = 10$ tree are up, and one creates a kink. We call n_0 the number of generations involved in the kink. If $n_0 = 1$, the kink has only one spin, if $n_0 = 2$, the kink has 7 spins, etc. We follow the magnetization of this domain as a function of time. The unit time is one Monte Carlo Step (MCS). One MCS corresponds to repeating N times the process which consists in choosing one spin at random among the N sites, and changing or not changing its direction, according to the Boltzmann distribution. The curves are averaged over 50 different Monte Carlo runs of the dynamics.

to the fact that the initial state is not thermalized; the thermalization occurs at small time scales compared to the collective processes of crossing the barrier. We define the typical relaxation time τ as the time scale associated with the vanishing of the magnetization. In figure 11 we have plotted the logarithm of this relaxation time, $\ln \tau$, as a function of the number of generations n_K in a kink K. The points are approximately aligned, indicating that the Arrhenius law

$$\tau \sim \tau_0 \exp\left(\beta\lambda \frac{z-2}{2} n\right) \tag{59}$$

is well satisfied. The case $\lambda = 1$ corresponds to the relaxation of an n-half-space tree where the ancestor is free. However, in our case, the ancestor is *not* free since the domain K is connected to the remaining up spins. The barrier height is essentially the same as in the case $\lambda = 1$, but the number of paths to reverse the magnetization is changed.

7.2. AC susceptibility

Experimentally, the AC nonlinear susceptibility has been a very useful probe of glassiness [26] since the third-order susceptibility couples to the Edwards–Anderson order parameter, and we can apply the same techniques numerically to study the tree problem that we are discussing here. In parallel with what is done experimentally, a small AC external field $H(t) = h \sin \omega t$ is applied to the spin system, and we measure the magnetization response, expanded into its Fourier components

$$M(\omega, t) = \sum_{k \geqslant 0} \theta'_k \sin k\omega t + \theta''_k \cos k\omega t \tag{60}$$

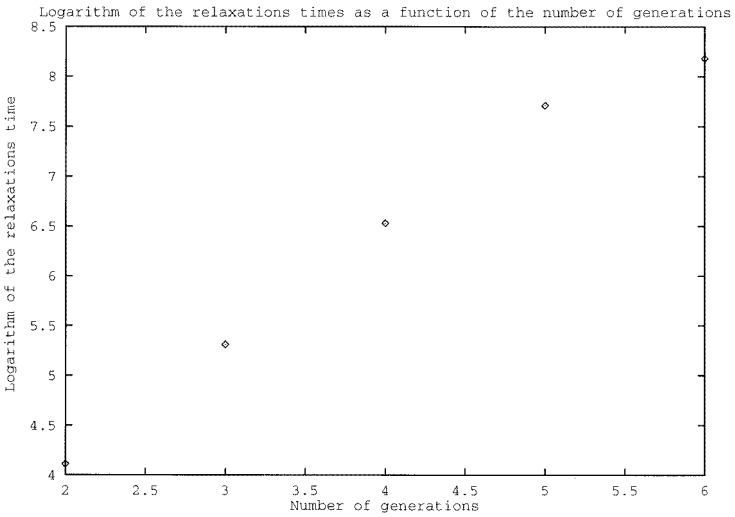

Figure 11. Logarithm of the relaxation time as a function of the number of generations in the kink. The relaxation time is defined from the cancellation of magnetization on figure 10. The points are approximately aligned, which is in agreement with the Arrhenius law of equation (59).

which has only odd harmonics. In practice, we let the system relax for four periods and we take measurements only during the fifth one. The in-phase susceptibilities are related to the in-phase Fourier coefficients as [26]

$$\theta_1' = \chi_1' h + \tfrac{3}{4}\chi_3' h^3 + \tfrac{5}{8}\chi_5' h^5 + \tfrac{35}{64}\chi_7' h^7 + \cdots \tag{61}$$

$$\theta_3' = \tfrac{1}{4}\chi_3' h^3 + \tfrac{5}{16}\chi_5' h^5 + \tfrac{21}{64}\chi_7' h^7 + \cdots \tag{62}$$

$$\theta_5' = \tfrac{1}{16}\chi_5' h^5 + \tfrac{7}{64}\chi_7' h^7 + \cdots \tag{63}$$

$$\theta_7' = \tfrac{1}{64}\chi_7' h^7 + \cdots. \tag{64}$$

Since *all* the nonlinear susceptibilities are divergent at the critical temperature of a spin glass [26], we must include all the measurable higher-order harmonics in order to properly include their influence on the lower ones [26].

The susceptibilities χ_1' and χ_3' are plotted as a function of temperature in figures 12 and 13 respectively for a number of frequencies. Both χ_1' and χ_3' display maxima, where that of the latter is more pronounced; in a 'real' spin glass in the thermodynamic limit one would expect χ_1' to have a maximum, and χ_3' to diverge. We note that χ_3' is negative near its maximum, which agrees with experiments on spin glasses [26]. The frequency dependence of the position of the maximum in χ_1' and χ_3' is also consistent with experiment [26], since the temperature for which χ_1' and χ_3' are maximum increases with frequency. Thus this study strongly suggests that the Ising model on a finite Cayley tree exhibits glassy-like behaviour at low temperatures; we shall be more specific when we analyse the Edwards–Anderson susceptibility of this model.

7.3. Autocorrelation functions and ageing

A good test used to determine the presence of glassiness in a given model involves the computation of the autocorrelation functions [27] to determine whether they exhibit ageing. Ageing is the signature of memory effects and broken ergodicity. The autocorrelation

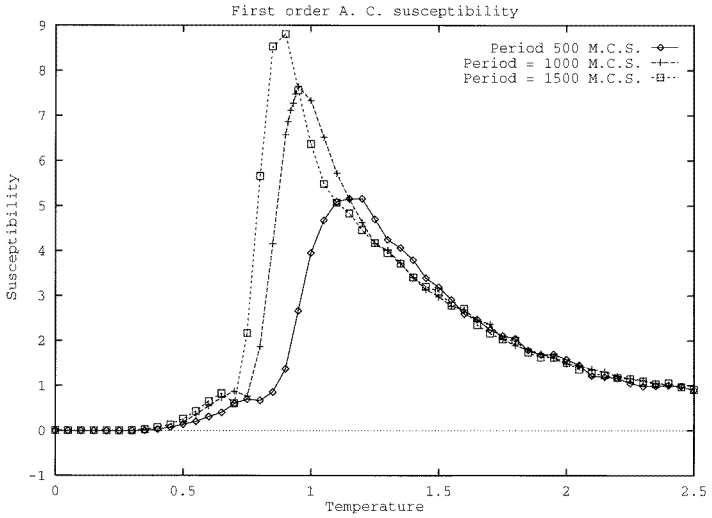

Figure 12. χ_1' susceptibility on the Cayley tree. The tree has 10 generations. The amplitude of the magnetic field is 0.1. The curves are averaged over 50 initial configurations of spins, generated at equilibrium. One has to find a compromise between the amplitude of the magnetic field and the number of configurations to be averaged over, to have a good signal/noise ratio. The curves correspond to a period of the magnetic field equal to 500 MCS, 1000 MCS and 1500 MCS.

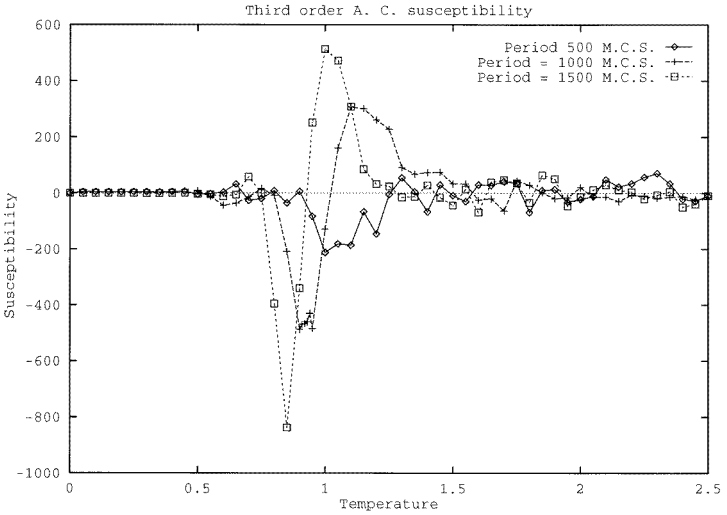

Figure 13. χ_3' susceptibility on the Cayley tree. The tree has 10 generations. The amplitude of the magnetic field is 0.1. The curves are averaged over 50 initial configurations of spins, generated at equilibrium. The curves correspond to a period of the magnetic field equal to 500 MCS, 1000 MCS and 1500 MCS.

functions are

$$C(t,t_w)=\frac{1}{N}\sum_{i=1}^{N}\langle\sigma_i(t+t_w)\sigma_i(t_w)\rangle-\langle\sigma_i(t+t_w)\rangle\langle\sigma_i(t_w)\rangle \tag{65}$$

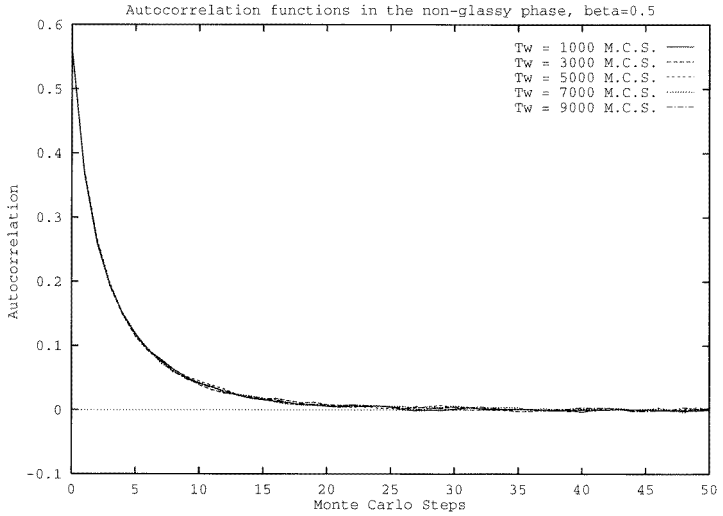

Figure 14. Spin autocorrelation functions of the $z = 3$ Cayley tree above T_g. The unit time is one MCS, the inverse temperature is $\beta = 0.5$, and the averages are taken over 100 random initial configurations. The autocorrelation functions decrease rapidly with t and are independent of t_w.

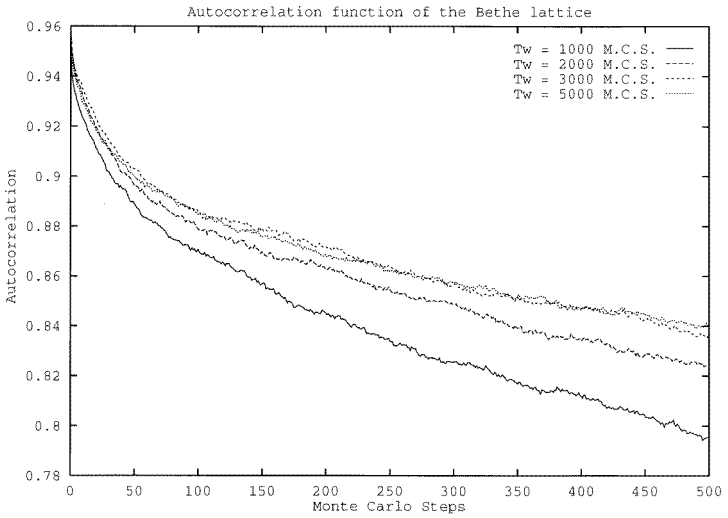

Figure 15. Spin autocorrelation functions of the $z = 3$ Cayley tree below T_g. The unit time is one MCS, the inverse temperature is $\beta = 2$ and the averages are taken over 100 random initial configurations. The autocorrelation functions depend on the waiting time, and *increase* with the waiting time, which is the signature of glassiness.

where the sample is rapidly quenched below T_g from a disordered high-temperature state. The Monte Carlo dynamics runs from times $t = 0$ to $t = t_w$; the autocorrelations are measured at $t = t_w$ where an average is taken over the initial configurations.

The autocorrelations in the high-temperature phase are plotted on figure 14. They decrease rapidly with the time t and are independent of the waiting time, as expected; this

is simply a check of our code. Figure 15 represents the autocorrelation functions below T_g. The autocorrelations *increase* with increasing t_w, indicating the presence of ageing. Such behaviour has been observed in a wide class of glassy models, including the fully frustrated hypercubic model [27].

8. The Edwards–Anderson order parameter and susceptibility

We have thus shown the existence of metastability and long time scales, and the existence of glassiness. It is thus interesting to study the Edwards–Anderson order parameter and susceptibility. The recursive structure of the Cayley tree permits us to compute the Edwards–Anderson order parameter and susceptibility at all temperatures. This calculation has already been done for the $\pm J$ model with uncorrelated boundary conditions in [10, 14]. These authors found an Almeida–Thouless line for their spin glass model, and we wish to use the same technique to analyse the model discussed here. In order to compute the Edwards–Anderson order parameter and susceptibility, we consider one tree plus one replica, with an inter-replica coupling R. If $\{\sigma\}$ and $\{\sigma'\}$ are the spin configurations of the two replicas, the Hamiltonian reads

$$H = -J\sum_{\langle i,j\rangle}(\sigma_i\sigma_j + \tilde{\sigma}_i\tilde{\sigma}_j) - R\sum_{i=1}^{N}\sigma_i\tilde{\sigma}_i + h\sum_{i=1}^{N}(\sigma_i + \tilde{\sigma}_i). \tag{66}$$

As usual with free boundary trees, we have to distinguish between the properties of the central spin and the whole tree; in what follows we discuss both cases below.

8.1. The whole tree

The partition function can be calculated by the construction of figure 2, even in the presence of the inter-replica coupling. We take derivatives of the partition function with respect to the inter-replica coupling, R, resulting in the Edwards–Anderson order parameter

$$q_{EA} = \frac{1}{N}\left\langle\sum_{i=1}^{N}\sigma_i\tilde{\sigma}_i\right\rangle = \frac{1}{N}\frac{\partial}{(\partial\beta R)}\ln Z(R=0) \tag{67}$$

and the Edwards–Anderson susceptibility

$$\chi_{EA} = \frac{1}{N}\left(\left\langle\left(\sum_{i=1}^{N}\sigma_i\tilde{\sigma}_i\right)^2\right\rangle - \left\langle\sum_{i=1}^{N}\sigma_i\tilde{\sigma}_i\right\rangle^2\right) = \frac{1}{N}\frac{\partial}{\partial(\beta R)^2}\ln Z(R=0). \tag{68}$$

We now let $Z^{(n)}_{\sigma\sigma'}$ be the conditional partition function of an n-half-space tree with respect to the ancestor's spins σ and σ'. It is clear that

$$Z^{(n+1)}_{++} = \mathrm{e}^{\beta R}\mathrm{e}^{2\beta H}(\mathrm{e}^{2\beta J}Z^{(n)}_{++} + Z^{(n)}_{+-} + Z^{(n)}_{-+} + \mathrm{e}^{-2\beta J}Z^{(n)}_{--})^{z-1} \tag{69}$$

$$Z^{(n+1)}_{+-} = \mathrm{e}^{-\beta R}(Z^{(n)}_{++} + \mathrm{e}^{2\beta J}Z^{(n)}_{+-} + \mathrm{e}^{-2\beta J}Z^{(n)}_{-+} + Z^{(n)}_{--})^{z-1} \tag{70}$$

$$Z^{(n+1)}_{-+} = \mathrm{e}^{-\beta R}(Z^{(n)}_{++} + \mathrm{e}^{-2\beta J}Z^{(n)}_{+-} + \mathrm{e}^{2\beta J}Z^{(n)}_{-+} + Z^{(n)}_{--})^{z-1} \tag{71}$$

$$Z^{(n+1)}_{--} = \mathrm{e}^{\beta R}\mathrm{e}^{-2\beta H}(\mathrm{e}^{-2\beta J}Z^{(n)}_{++} + Z^{(n)}_{+-} + Z^{(n)}_{-+} + \mathrm{e}^{2\beta J}Z^{(n)}_{--})^{z-1}. \tag{72}$$

The initial conditions of the recursion are $Z^0_{++} = \mathrm{e}^{\beta R}\mathrm{e}^{2\beta H}$, $Z^0_{+-} = Z^0_{-+} = \mathrm{e}^{-\beta R}$ and $Z^0_{--} = \mathrm{e}^{\beta R}\mathrm{e}^{-2\beta H}$. For all n, we can show that $Z^{(n)}_{+-} = Z^{(n)}_{-+}$ and we then define $Z^{(n)}_1 \equiv Z^{(n)}_{++}$, $Z^{(n)}_0 \equiv Z^{(n)}_{+-} = Z^{(n)}_{-+}$ and $Z^n_{-1} \equiv Z^{(n)}_{--}$. Using this notation, the recursion relations become

$$Z^{(n+1)}_1 = \mathrm{e}^{\beta(R+2H)}(\mathrm{e}^{2\beta J}Z^{(n)}_1 + 2Z^{(n)}_0 + \mathrm{e}^{-2\beta J}Z^{(n)}_{-1})^{z-1} \tag{73}$$

$$Z_0^{(n+1)} = \mathrm{e}^{-\beta R}(Z_1^{(n)} + 2\cosh\beta J Z_0^{(n)} + Z_{-1}^{(n)})^{z-1} \tag{74}$$

$$Z_{-1}^{(n+1)} = \mathrm{e}^{\beta(R-2H)}(\mathrm{e}^{-2\beta J} Z_1^{(n)} + 2Z_0^{(n)} + \mathrm{e}^{2\beta J} Z_{-1}^{(n)})^{z-1} \tag{75}$$

which can be used to obtain q_{EA} and χ_{EA} in a straightforward fashion. q_{EA} and χ_{EA} are plotted in figures 16 and 17 respectively for $n = 10$ and $n = 80$. In both cases, the curves corresponding to these two system sizes are similar, even though the number of sites is small for $n = 10$ (2047 sites) and macroscopic for $n = 80$ (4.02 moles of sites). We believe that this behaviour is related to the very slow variation of the glass temperature T_g with the system size. In figure 17 we see clearly that χ_{EA} does not diverge in the thermodynamic limit but rather exhibits a maximum, characteristic of a finite-size effect, even in the macroscopic regime.

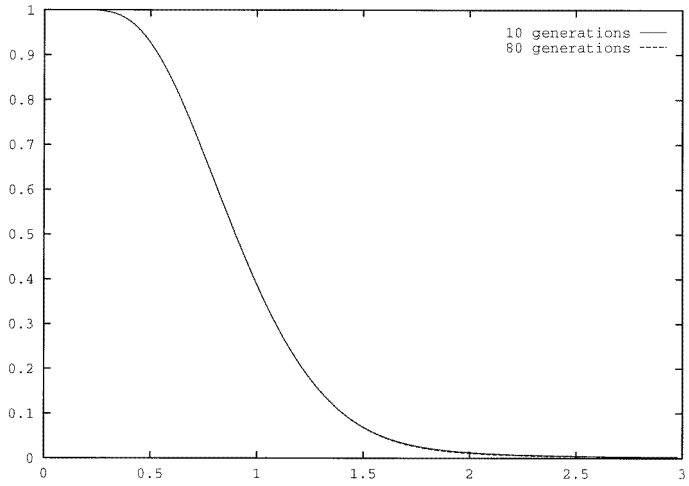

Figure 16. Edwards–Anderson order parameter for the whole spin system. The coordination is $z = 3$. The Edwards–Anderson order parameter is plotted as a function of temperature for $n = 10$ (2047 spins) and $n = 80$ (4.02 moles of spins). The two curves nearly coincide.

8.2. The central spin

Following the authors of [10, 14], we note that

$$Z^{(n)} = Z_1^{(n)} + 2Z_0^{(n)} + Z_{-1}^{(n)} \tag{76}$$

$$Q^{(n)} = \frac{1}{Z^{(n)}}(Z_1^{(n)} - 2Z_0^{(n)} + Z_{-1}^{(n)}). \tag{77}$$

The Edwards–Anderson order parameter of the central spin is $\tilde{q}_{EA} = Q^{(n)}/Z^{(n)}$, and the Edwards–Anderson susceptibility is

$$\tilde{\chi}_{EA}^{(n)} = \frac{\partial \tilde{q}_{EA}}{(\partial\beta R)}(R = 0) \tag{78}$$

where the tilde symbol denotes quantities with respect to the central spin. The 'central spin' Edwards–Anderson susceptibility $\tilde{\chi}_{EA}$ is plotted in figure 18 for various system sizes. Though we have seen that finite-size effects are negligible for the whole tree, they become crucial for the central spin. More specifically, the maximum values of the Edwards–Anderson susceptibility of the central spin does not increase (see figure 19) as a function of

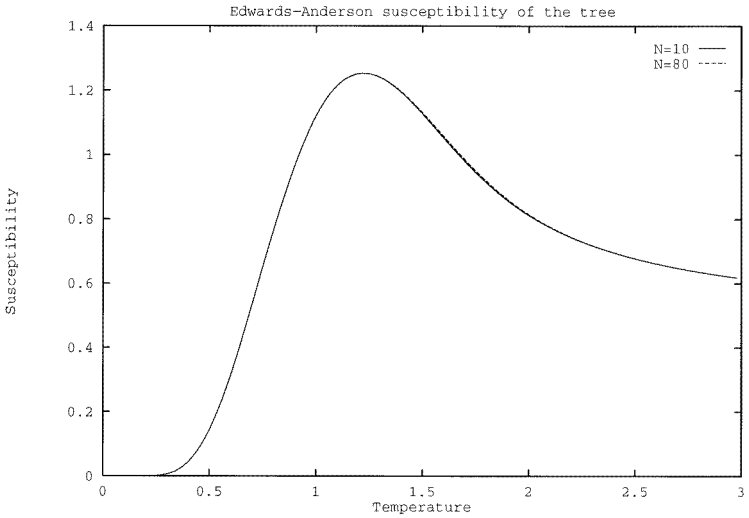

Figure 17. Edwards–Anderson susceptibility for the whole spin system. The coordination is $z = 3$. The Edwards–Anderson susceptibility is plotted as a function of temperature for $n = 10$ (2047 spins) and $n = 80$ (4.02 moles of spins). The two curves nearly coincide.

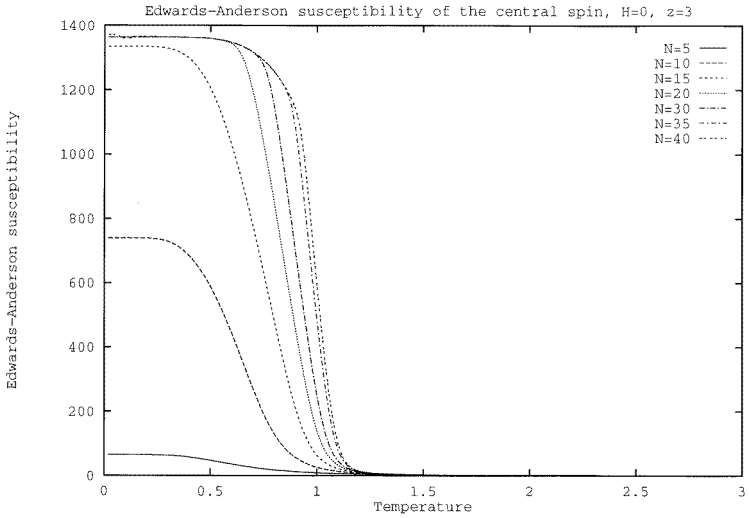

Figure 18. Edwards–Anderson susceptibility for the central spin as a function of temperature for $n = 5$, 10, 15, 20, 25, 30, 35, 40 generations. The coordination $z = 3$.

coordination z. As the system size becomes macroscopic, the glass temperature T_g depends more on the coordination than on the number of generation; in particular, it increases with increasing coordination consistent with equation (15).

8.3. Central spin in a magnetic field

In the Sherrington–Kirkpatrick model, glassy behaviour persists even in the presence of a magnetic field; the Edwards–Anderson susceptibility diverges with an exponent $\gamma = 1$

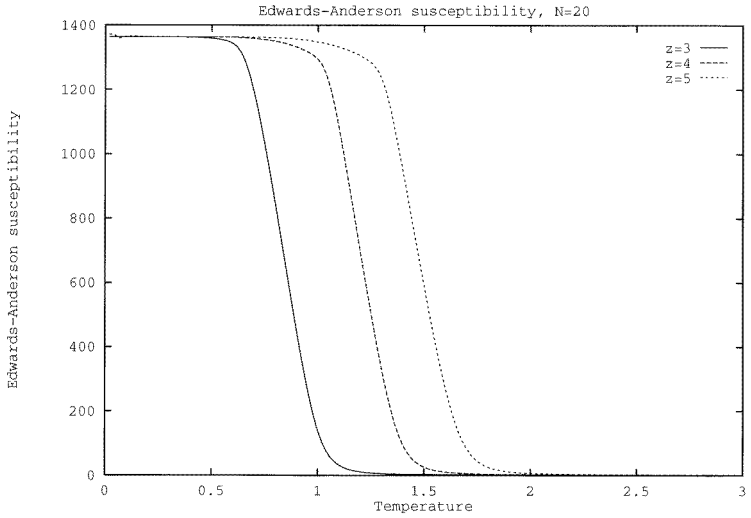

Figure 19. Edwards–Anderson susceptibility for the central spin as a function of temperature for $z = 3, 4, 5$. The number of generations is $n = 20$.

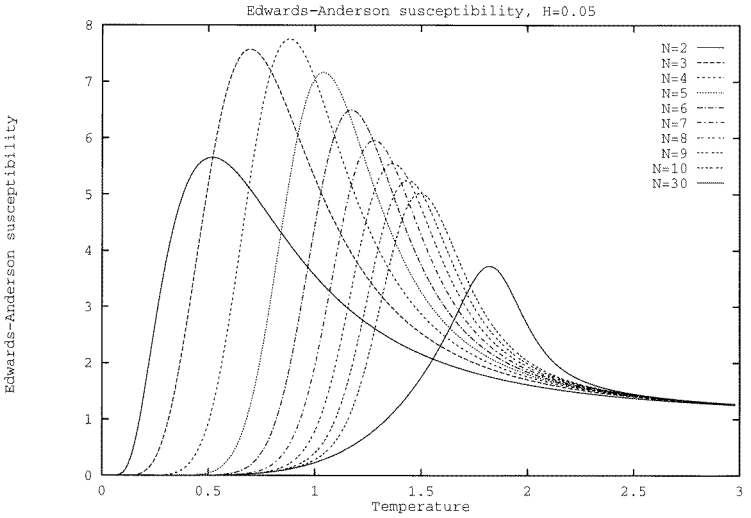

Figure 20. Edwards–Anderson susceptibility of the central spin in a magnetic field as a function of temperature, for different sizes. The number of generations is $n = 2, 3, 4, 5, 6, 7, 8, 9, 10, 30$. The magnetic field is $H = 0.05$.

through the Almeida–Thouless line. We have studied the behaviour of the Ising NN ferromagnet (FM) on a Cayley tree ferromagnetic model with free boundary conditions with an applied magnetic field. Specifically we studied the variation of the Edwards–Anderson susceptibility in a field as a function of system size. As displayed in figure 20, the maximum of the Edwards–Anderson susceptibility as a function of temperature depends on the size. In figure 21, we show the locus of the maxima of $\tilde{\chi}_{EA}$ for different magnetic fields as a function of temperature. The Edwards–Anderson susceptibility decreases strongly with increasing magnetic field, indicating the vanishing of glassy behaviour consistent with the

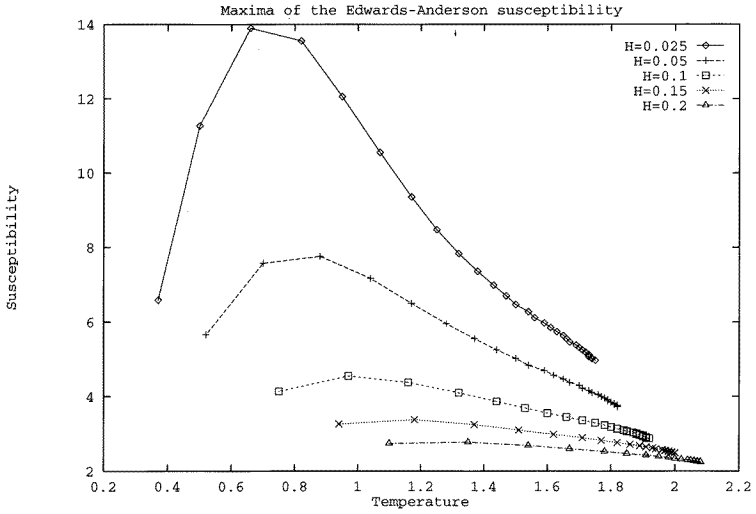

Figure 21. Maxima of χ_{EA} as a function of temperature for different values of the magnetic field. The system size is $n = 10$ generations. The magnetic fields are $H = 0.025$, $H = 0.05$, $H = 0.1$, $H = 0.15$, $H = 0.2$.

exponential decay of the cross over magnetic field of equation (B28), and also with the fact that the local maxima of the magnetization distribution in a magnetic field disappear very rapidly as a magnetic field is switched on (see figure 5).

9. Discussion

In summary, we have studied the static and the dynamical properties of the nearest-neighbour Ising model on a Cayley tree. At zero field, we find that this system displays glassy behaviour below a size-dependent temperature that scales inversely with the logarithm of the number of generations; thus its glassy behaviour persists for a finite but macroscopic number of sites. Because the ratio of the number of surface to bulk sites, N_s/N, and the strength of the external field, h, play a key role in the physical behaviour of the resident spin system, the different thermodynamic limits associated with the values of N_s/N and h are characterized; the crossover temperature, T_g, is associated with fixed N_s/N in the limit of vanishing applied field. Physically well-defined large domains of flipped spins develop at T_g; at this temperature the probability of nested spin clusters is small. The largest energy barriers associated with overturning these domains is determined to scale logarithmically with the number of sites at zero temperature, a result that should be valid at finite, low temperatures if overlap between spin clusters does not occur. A dynamical study indicates the appearance of metastable states and long relaxation times at low temperatures. The autocorrelations are computed after a waiting time using Monte Carlo dynamics; they exhibit ageing for $T < T_g$. The temperature variations of the coefficients of χ_1' and χ_3' are also determined and they agree with the existence of finite-size glassiness. Finally the Edwards–Anderson susceptibility of the entire tree displays a maximum (but no divergence) that evolves slowly with increasing system size; that of the central spin has much more marked size-dependence.

We have thus performed a detailed characterization of the low-temperature phase of a short-range periodic spin model resident on a Cayley tree. In this particular case, we have

found that it displays finite-size glassy behaviour that remains for a macroscopic number of sites; perhaps it is best to characterize this low-temperature phase as a very viscous spin liquid. We note that neither intrinsic disorder nor frustration exist due to the initial Ising Hamiltonian; the possibility of many low-temperature 'cluster' states separated by very high energy barriers is a direct consequence of the unusual topology of the Cayley tree. In many ways we hope that this is a warm-up exercise towards the study of spin models on more complicated non-Euclidean lattices, e.g. on a constant triangulation associated with a surface of negative curvature, where the intrinsic geometry of the host may lead to the possibility of glassiness in the absence of both disorder and frustration.

Appendix A

We propose another derivation of the magnetization distribution for the tree. Let $Z(\beta, h)$ be the partition function of the spin system in the presence of an external field. Then

$$P(M) = \frac{1}{Z(\beta,h)} \sum_{\{\sigma\}} \delta\left(M - \sum_{i=1}^{N} \sigma_i\right) \exp\left(\beta\left(J \sum_{\langle i,j\rangle} \sigma_i\sigma_j + h \sum_{i=1}^{N} \sigma_i\right)\right). \tag{A1}$$

Using the Fourier representation of the delta function

$$\delta\left(M - \sum_{i=1}^{N} \sigma_i\right) = \frac{1}{2\pi} \int_0^{2\pi} \mathrm{d}\lambda\, \mathrm{e}^{\mathrm{i}\lambda M} \mathrm{e}^{-\mathrm{i}\lambda \sum_{i=1}^{N} \sigma_i} \tag{A2}$$

we obtain

$$P(M) = \frac{1}{2\pi} \int_0^{2\pi} \mathrm{d}\lambda \mathrm{e}^{\mathrm{i}\lambda M} \frac{Z(\beta, h - \mathrm{i}\lambda/\beta)}{Z(\beta,h)} \tag{A3}$$

where we have used the analytic continuation of the partition function for complex magnetic fields. This method is useful provided one knows how to calculate the partition function, which is certainly feasible on a tree. We proceed by decimation, starting from the border of the n-half-space tree. For future purposes, we denote $Z_n(\beta, h, h_n)$ the partition function of an n-half-space tree with a magnetic field h acting on the spins of the generations 0 to $n-1$, and h_n on the spins of the generation n. We first consider the situation where $z-1$ spins $\sigma_1, \ldots, \sigma_{z-1}$ are connected to an ancestor Σ. An external field h_n acts on the spins σ_i. The partition function of this system is

$$z(\Sigma) = \left(\sum_{\sigma} \mathrm{e}^{\beta J \Sigma\sigma} \mathrm{e}^{\beta h_n \sigma}\right)^{z-1}. \tag{A4}$$

The summations over σ_i have been factored out since there are no loops. We next write $z(\Sigma)$ under the form $z(\Sigma) = \mathcal{N} \exp(\beta T h_n)$. Since there are two equations (one for $\Sigma = 1$ and one for $\Sigma = -1$) for two parameters ($\mathcal{N}$ and h), the parameters $\mathcal{N}$ and Th_n exist, are unique, and are determined by

$$\mathcal{N}^2 = z(+)z(-) = (4(\cosh^2(\beta J) + \sinh^2(\beta h_n)))^{z-1} \tag{A5}$$

$$Th_n = \frac{1}{2\beta} \ln\left(\frac{z(+)}{z(-)}\right) = \frac{z-1}{2\beta} \ln\left(\frac{\cosh(\beta(J+h_n))}{\cosh(\beta(J-h_n))}\right). \tag{A6}$$

Coming back to the partition function on the Cayley tree, we have

$$Z_n(\beta, h, h_n) = (4(\cosh^2(\beta J) + \sinh^2(\beta h_n)))^{(z-1)^{n-1}/2} Z_{n-1}(\beta, h, h + Th_n). \tag{A7}$$

The last term of the recursion corresponds to the partition function of the ancestor, which is simply

$$Z_1(\beta, h) = 2\cosh(\beta T^n h). \tag{A8}$$

It is straightforward to compute the partition function using these relations and to perform the Fourier transform (A3) in order to obtain the probability distribution of the magnetization.

Appendix B

We present here the calculations corresponding to section 2.2. Details of the calculation of the partition function are given in appendix A, and we obtain

$$\langle M(n,m,h)\rangle = \sum_{i=n-m}^{n-1} (z-1)^{n-i} \frac{\sin\beta h_i \cosh\beta h_i}{\cosh^2\beta J + \sinh^2\beta h_i} \frac{\mathrm{d}h_i}{\mathrm{d}\lambda}(\lambda = 0) + \tanh\beta h_n \frac{\mathrm{d}h_n}{\mathrm{d}\lambda}(\lambda = 0). \tag{B1}$$

The last term is the contribution of the ancestor to the average magnetization; h_i is the total field at generation i which is the sum of the external, the source and the recursive (of (5) fields (h, λ and h^{ind}) respectively).

We do not treat the iteration of h^{ind} exactly, but approximate it as described below. From the iteration (5) we can deduce the shape of h_{i+1}^{ind} as a function of h_i, which is plotted in figure 3. If $\beta < \beta_c$, the slope at the origin is less than unity, whereas it is larger than unity for $\beta > \beta_c$. Moreover for $\beta > \beta_c$ there is one non-trivial fixed point, for which $h_{i+1}^{ind} = h_i = h^*$ which depends only on the temperature. This behaviour suggests that the iteration can be approximated by linearizing $h_{i+1}(h_i)$ in the vicinity of $h_i = 0$ and of $h_i = h^*$. More precisely, we deduce from (5) that

$$\frac{\mathrm{d}h_{i+1}^{ind}}{\mathrm{d}h_n} = (z-1)\frac{\sinh\beta J \cosh\beta J}{\cosh^2\beta J + \sinh^2\beta h_i} \tag{B2}$$

and define new variables, η_1 and η_2, such that

$$\frac{\mathrm{d}h_{i+1}^{ind}}{\mathrm{d}h_i}(h_i = 0) = (z-1)\tanh\beta J \equiv 1 + \eta_1 \tag{B3}$$

$$\frac{\mathrm{d}h_{i+1}^{ind}}{\mathrm{d}h_i}(h_i = h^*) \equiv 1 - \eta_2 \tag{B4}$$

where $\eta_1 \in [0, z-2]$ and $\eta_2 \in [0,1]$ and we note that η_1 and η_2 depend only on the temperature. We then express the complete recursion by

$$h_{i+1}^{ind} = (1+\eta_1)h_i \tag{B5}$$

or

$$h_{i+1}^{ind} = \eta_2 h^* + (1-\eta_2)h_i. \tag{B6}$$

The first linearization corresponds to $h_i \in [0, h_c]$ and the second one to $h_i \in [h_c, h^*]$, where

$$h_c = \frac{\eta_2}{\eta_1 + \eta_2} h^*. \tag{B7}$$

If $\lambda = 0$, iteration of the total magnetic field h_n leads to different results depending on the relative magnitude of i (generation) compared with

$$n_c(h) = \left[\frac{1}{\ln(1+\eta_1)} \ln\left(\frac{\eta_1\eta_2}{\eta_1+\eta_2}\frac{h^*}{h} + 1\right)\right] \tag{B8}$$

where [] denotes the integer part; for $i \leqslant n_c(h)$

$$h_i = \frac{h}{\eta_1}((1+\eta_1)^{i+1} - 1) \tag{B9}$$

and if $i \geqslant n_c(h)$

$$h_i = h^* + \frac{h}{\eta_2} + \left(h_{n_c} - h^* - \frac{h}{\eta_2}\right)(1-\eta_2)^{i-n_c}. \tag{B10}$$

There are therefore three regimes which we can study corresponding to the application of large (I), intermediate (II) and vanishing (III) fields on the finite Cayley tree; more specifically they correspond to the conditions $0 \leqslant n_c \leqslant n-m$ (I), $n-m+1 \leqslant n_c \leqslant n$ (II) and $n_c \geqslant n$ (III), respectively, where n_c is defined in equation (B8).

Appendix B.1. Regime I: $0 \leqslant n_c \leqslant n-m$—large fields

We now determine the average magnetization as given by equation (B1) in regime I. Using the approximation discussed in the previous section, we write

$$\frac{\mathrm{d}h_i}{\mathrm{d}\lambda}(\lambda = 0) = \frac{1}{\eta_2}(1 - (1-\eta_2)^{i-n+m+1}). \tag{B11}$$

If $0 \leqslant h_i \leqslant h_c$ or $i < n_c$, we can approximate

$$\frac{\sinh \beta h_i \cosh \beta h_i}{\cosh^2 \beta J + \sinh^2 \beta h_i} \simeq a_1 h_i \tag{B12}$$

where

$$a_1 = \frac{\beta}{\cosh^2 \beta J} \tag{B13}$$

and if $h_i \geqslant h_c$ or $n \geqslant n_c$, we use

$$\frac{\sinh \beta h_i \cosh \beta h_i}{\cosh^2 \beta J + \sinh^2 \beta h_i} \simeq a_2(h_i - h^*) + b_2 \tag{B14}$$

where

$$a_2 = \frac{\cosh^2 \beta J \cosh^2 \beta h^* + \sinh^2 \beta J \sinh^2 \beta h^*}{(\cosh^2 \beta J + \sinh^2 \beta h^*)^2} \tag{B15}$$

$$b_2 = \beta \frac{\sinh \beta h^* \cosh \beta h^*}{\cosh^2 \beta J + \sinh^2 \beta h^*}. \tag{B16}$$

It is now straightforward to insert these expressions into equation (B1) for the average magnetization. Since we normalize by the number of sites

$$N_m = 1 + (z-1) + \cdots + (z-1)^m = \frac{(z-1)^{m+1} - 1}{z-2} \tag{B17}$$

it is reasonable to neglect the contribution of the ancestor. We obtain

$$\begin{aligned}\langle M(n,m,h)\rangle = \frac{1}{\eta_2}\Bigg[&\left(b_2 + a_2\frac{h}{\eta_2}\right)N_m + (z-1)^m \frac{1 - ((1-\eta_2)/(z-1))^m}{1 - ((1-\eta_2)/(z-1))} \\ &\left(-\left(b_2 + a_2\frac{h}{\eta_2}\right)(1-\eta_2) + a_2(h_{n_c} - h_\infty)(1-\eta_2)^{n-m-n_c}\right) \\ &- a_2(h_{n_c} - h_\infty)(z-1)^m(1-\eta_2)^{n-m-n_c+1}\frac{1 - ((1-\eta_2)^2/(z-1))^m}{1 - ((1-\eta_2)^2/(z-1))}\Bigg]\end{aligned} \tag{B18}$$

where $h_\infty = h^* + h/\eta_2$. We can now discuss the different thermodynamic limits. First we note that if $n \to \infty$, $m \to \infty$ and $n - m \to \infty$, the thermodynamic limit of the normalized magnetization reads

$$\lim \frac{\langle M(n,m,h)\rangle}{N_m} = \left(b_2 + a_2\frac{h}{\eta_2}\right)\frac{z-1}{z-2+\eta_2}. \tag{B19}$$

However, if we take a *different* thermodynamic limit, with $n-m \to b$, where b is a constant thickness boundary, we obtain

$$\lim \frac{\langle M(n,m,h)\rangle}{N_m} = \left(b_2 + a_2\frac{h}{\eta_2}\right)\frac{z-1}{z-2+\eta_2} - a_2(h_\infty - h_{n_c})\frac{(z-1)(z-2)(1-\eta_2)^{b-n_c}}{(z-2+\eta_2)(z-1-(1-\eta_2)^2)} \tag{B20}$$

where $b = n - n_c + 1$. The absolute value of the corrective term decreases as the thickness of the boundary increases since $|1-\eta_2| < 1$.

Appendix B.2. Regime II: $n - m + 1 \leqslant n_c \leqslant n$—intermediate fields

Again we calculate the average magnetization (B1) this time in the regime $n-m+1 \leqslant n_c \leqslant n$ where we use the relations (B12) and (B14) from the previous section. Furthermore we need to approximate the expression $\mathrm{d}h_i/\mathrm{d}\lambda$ for $\lambda = 0$. If $n - m \leqslant i \leqslant n_c$, we have

$$\frac{\mathrm{d}h_i}{\mathrm{d}\lambda}(\lambda = 0) = \frac{1}{\eta_1}((1+\eta_1)^{i-n+m+1} - 1) \tag{B21}$$

and if $i \geqslant n_c$,

$$\frac{\mathrm{d}h_i}{\mathrm{d}\lambda}(\lambda = 0) = \frac{1}{\eta_2} + a(1-\eta_2)^{i-n_c} \tag{B22}$$

where

$$a = \frac{1}{\eta_1}(1+\eta_1)^{n_c-n+m+1} - \frac{1}{\eta_1} - \frac{1}{\eta_2}. \tag{B23}$$

We have used

$$h_i = h^* + \frac{h+\lambda}{\eta_2} + (1-\eta_2)^{i-n_c}\left(h_{n_c}(\lambda) - h^* - \frac{h+\lambda}{\eta_2}\right) \tag{B24}$$

with

$$h_{n_c}(\lambda) = h_{n_c}(0) + \frac{\lambda}{\eta_1}((1+\eta_1)^{n_c-n+m+1} - 1). \tag{B25}$$

We insert these expressions into (B1) and sum the full geometric series. We note that the thermodynamic limit can only be taken with $n - m \to b$, where again b is a constant. We find that the dominant behaviour at small magnetic field h depends on the temperature. Let T' be the temperature such that $\tanh\beta' J = 1/\sqrt{z-1}$. Then if $T' < T < T_c$ the dominant term in the normalized magnetization is linear in h with corrections in h^α, where $\alpha = \ln(z-1)/\ln(1+\eta_1) - 1$; by contrast if $T < T'$ the leading term is of order h^α. We do not write explicitly the corresponding expressions since they are tedious and do not contribute further to the present discussion.

Appendix B.3. Regime III: $n_c \geqslant n$—vanishing fields

In this regime, we approximate the average magnetization by inserting (B12) and (B21) into (B1) which yields

$$\langle M(n,m,h)\rangle = \sum_{i=n-m}^{n-1} (z-1)^{n-i} a_1 h \frac{(1+\eta_1)^{i+1}-1}{\eta_1} \frac{(1+\eta_1)^{i-n+m+1}-1}{\eta_1}. \tag{B26}$$

After summing the geometrical series, we obtain

$$\begin{aligned}\frac{\langle M(n,m,h)\rangle}{N(m)} = {} & \frac{a_1 h}{\eta_1^2} \frac{z-2}{1-(z-1)^{-m-1}} \\ & \times \left[\frac{1-(z-1)^{-m}}{z-2} - \frac{(1+\eta_1)((1+\eta_1)^b+1)}{z-2-\eta_1} \left(1-\left(\frac{1+\eta_1}{z-1}\right)^m\right) \right. \\ & \left. + \frac{(1+\eta_1)^{b+2}}{(1+\eta_1)^2-z+1} \left(-1+\left(\frac{(1+\eta_1)^2}{z-1}\right)^m\right)\right].\end{aligned} \tag{B27}$$

We identify the crossover field h_{co} as $h_{n-1} = h_c$, that is

$$h_{co} = h^* \frac{\eta_1 \eta_2}{(\eta_1+\eta_2)((1+\eta_1)^n-1)} \tag{B28}$$

which is exponentially small in n. If we take the limit of large n and m but finite $n-m$, we define the susceptibility per spin by

$$\frac{\langle M(n,m,h)\rangle}{N(m)} \sim h_\chi(m). \tag{B29}$$

If $T > T'$, where T' is defined by $\tanh(\beta' J) 1/\sqrt{z-1}$, the susceptibility per spin tends to a constant in the thermodynamic limit:

$$\chi(m) \to \frac{a_1(z-2)}{\eta_1^2} \left[\frac{1}{z-2} - \frac{(1+\eta_1)((1+\eta_1)^b+1)}{z-2-\eta_1} - \frac{(1+\eta_1)^{b+2}}{(1+\eta_1)^2-z+1} \right]. \tag{B30}$$

If $T < T'$, the susceptibility per spin diverges exponentially in the thermodynamic limit:

$$\chi(m) \sim \frac{a_1(z-2)(1+\eta_1)^{b+2}}{(1+\eta_1)^2-z+1} \left(\frac{(1+\eta_1)^2}{z-1}\right)^m \tag{B31}$$

so that the susceptibility per spin is proportional to

$$\chi(m) \propto N_m(1-4m\mathrm{e}^{-2\beta J}). \tag{B32}$$

Appendix C

In this appendix we give the value of the energy barrier $E(T_{n,z})$ for a half-space tree $T_{n,z}$ with n generations and a coordination number of z for all sites except the root (coordination $z-1$) and the leaves (coordination 1). We also give the energy barrier $E(T^*_{n,z})$ for a complete tree $T^*_{n,z}$ with n generations and a coordination number of z for all sites except the leaves. The derivation of the formula is due to Sebö and Preissmann, and is published *in extenso* in [28]. Note that the same problem arises in the VLSI circuit conception! Generically the problem of finding the lowest energy barrier is *NP-complete*, but the sub-problem of

finding the lowest energy barrier of a tree is polynomial, and an explicit algorithm is given hereafter. The value of the energy barriers is given by

$$\begin{aligned} E(T_{n,z}) &= \left\lceil \frac{n(z-2)}{2} \right\rceil + 1 \qquad (n, z \geqslant 3) \\ E(T^*_{n,z}) &= \left\lceil \frac{(n-1)(z-2)}{2} \right\rceil + \left\lceil \frac{z-2}{2} \right\rceil + 1 \qquad (n, z \geqslant 3). \end{aligned} \tag{C1}$$

In the above formula $\lceil x \rceil$ denotes the lowest of the integers greater than x. The demonstration of these formulae is constructive. Firstly a lower bound for E is given. Then an algorithm is described which produces a labelling of the sites. Flipping the spins in the order of this labelling gives an energy barrier exactly equal to the lower bound. The algorithm is recursive. It tries to produce an optimal labelling of the sites where the root is labelled *before* the configuration of highest energy is reached. We call such a labelling *strong* labelling. This extra constraint is useful when one applies z times the algorithm on a $T_{n,z}$ to compute $E(T_{n+1,z})$, or when one applies the algorithm to $T_{n,z}$ and to $T_{n-1,z}$ to compute $E(T^*_{n+1,z})$. A strong labelling does not exist when z and n are both odd as shown in [28]. Let us now consider the case of $T_{n,z}$. Formula (C1) means that

• when z is even the increment in energy when one goes from $T_{n,z}$ to $T_{n+1,z}$ is *constant* and equal to $\frac{z}{2} - 1$;

• when z is odd the increment in energy when one goes from $T_{n,z}$ to $T_{n+1,z}$ is *alternatively* $\frac{z-1}{2} - 1$ and $\frac{z-1}{2}$.

We give now the algorithm in the case of even z. The case of odd z is slightly more complicated, but in the same spirit. Consider $T_{n,z}$ as being made of $z-1$ copies of $T_{n-1,z}$, all of them connected to the site 0. Each spin is identified by two numbers k, i with $0 \leqslant k < z-1$ and $0 \leqslant i < N_{n-1}$ (N_n is the number of sites of $T_{n,z}$). Let us note π a strong labelling of $T_{n-1,z}$, and n_0 the root of the $(\frac{z-2}{2} - 1)$th copy of $T_{n-1,z}$. The following labelling is a strong labelling of $T_{n,z}$:

(i) $(0, \pi(0)), (0, \pi(1)), \ldots, (0, \pi(N_{n-1}))$
(ii) ...
(iii) $(\frac{z-2}{2} - 1, \pi(N_n)), (\frac{z-2}{2} - 1, \pi(N_n - 1)), \ldots, (\frac{z-2}{2} - 1, \pi(n_0))$
(iv) 0
(v) $(\frac{z-2}{2} - 1, \pi(n_0 - 1)), (\frac{z-2}{2} - 1, \pi(n_0 - 2)), \ldots, (\frac{z-2}{2} - 1, \pi(0))$
(vi) $(\frac{z-2}{2}, \pi(0)), (\frac{z-2}{2}, \pi(1)), \ldots, (\frac{z-2}{2}, \pi(N_{n-1}))$
(vii) ...
(viii) $(z-2, \pi(0)), (z-2, \pi(1)), \ldots, (z-2, \pi(N_{n-1}))$.

Note that in steps (i), (ii), (vii) and (viii) any admissible permutation can be used instead of the strong labelling π. It is shown in [28] that the above labelling is indeed an optimal labelling and it can be used to implement a recursive algorithm to find a path between the two ferromagnetic states.

References

[1] For a pedagogical review of recursive structures see Thorpe M F 1982 *Excitations in Disordered Solids (NATO Advanced Study Institute Series B)* ed M F Thorpe (New York: Plenum) pp 85–107
[2] Domb C 1960 *Adv. Phys.* **9** 145
[3] See, for example, Baxter R J 1982 *Exactly Solved Models in Statistical Mechanics* (London: Academic) ch 4
[4] Gujrati P D 1995 *Phys. Rev. Lett.* **74** 809
[5] Thouless D J, Anderson P W and Palmer R G 1977 *Phil. Mag.* **35** 593
[6] Sherrington D and Kirkpatrick S 1975 *Phys. Rev. Lett.* **35** 1792
[7] Bowman D and Levin K 1982 *Phys. Rev.* B **25** 3438

[8] Thouless D J 1986 *Phys. Rev. Lett.* **56** 1082
[9] Katsura S 1986 *Prog. Theor. Phys.* **87** 139
[10] Chayes J T, Chayes L, Sethna J P and Thouless D J 1986 *Commun. Math. Phys.* **106** 41
[11] Mottishaw P 1987 *Europhys. Lett.* **4** 333
[12] Pik-Yin Lai and Goldschmidt Y Y 1989 *J. Phys. A: Math. Gen.* **22** 399
[13] Carlson J M, Chayes J T, Chayes L, Sethna J P and Thouless D J 1990 *Europhys. Lett.* **5** 355; 1990 *J. Stat. Phys.* **61** 987
[14] Carlson J M, Chayes J T, Sethna J P and Thouless D J 1990 *J. Stat. Phys.* **61** 1069
[15] Goldschmidt Y Y 1991 *Phys. Rev.* B **43** 8148
[16] Gujrati P J 1984 *Phys. Rev. Lett.* **53** 2453; 1993 *J. Chem. Phys.* **98** 1613
[17] Stinchcombe R B 1973 *J. Phys. C: Solid State Phys.* **6** L1
[18] Rammal R 1985 *J. Physique* **46** 1837
Rammal R and Benoit A 1985 *J. Physique Lett.* **46** L667; 1985 *Phys. Rev. Lett.* **55** 649
[19] Swendsen R H and Wang J S 1986 *Phys. Rev. Lett.* **57** 2606; 1987 *Phys. Rev. Lett.* **58** 86
See also Swendsen R H, Wang J S and Ferrenberg A M 1992 *The Monte Carlo Method in Condensed Matter Physics (Topics in Applied Physics 71)* ed K Binder (Berlin: Springer)
[20] Eggarter T P 1974 *Phys. Rev.* B **9** 2989
[21] Matsuda M 1974 *Prog. Theor. Phys.* **51** 1053
[22] von Heimburg J and Thomas H 1974 *J. Phys. C: Solid State Phys.* **7** 3433
[23] Muller-Hartmann E and Zittartz J 1974 *Phys. Rev. Lett.* **33** 893
[24] Glauber R J 1963 *J. Math. Phys.* **4** 294
[25] Mélin R 1996 *J. Physique* I **6** 469
[26] Chalupa J 1977 *Solid State Commun.* **22** 315
Suzuki J 1977 *Prog. Theor. Phys.* **58** 1151
Lévy L P 1988 *Phys. Rev.* B **38** 4963
[27] Marinari E, Parisi G and Ritort F *Preprint* cond-mat/9410089
[28] Anglès d'Auriac J C, Preissmann M and Sebö A 1995 *J. Math. Combinatorics* submitted